AFRL-RX-WP-TR-2010-4167

COLLABORATIVE RESEARCH AND DEVELOPMENT (CR&D)

Delivery Order 0034: Aircraft Coatings Modeling and Simulation

Taner Dirama

Universal Technology Corporation

MARCH 2008
Final Report

STINFO COPY

AIR FORCE RESEARCH LABORATORY
MATERIALS AND MANUFACTURING DIRECTORATE
WRIGHT-PATTERSON AIR FORCE BASE, OH 45433-7750
AIR FORCE MATERIEL COMMAND
UNITED STATES AIR FORCE

NOTICE AND SIGNATURE PAGE

Using Government drawings, specifications, or other data included in this document for any purpose other than Government procurement does not in any way obligate the U.S. Government. The fact that the Government formulated or supplied the drawings, specifications, or other data does not license the holder or any other person or corporation; or convey any rights or permission to manufacture, use, or sell any patented invention that may relate to them.

This report was cleared for public release by the USAF 88th Air Base Wing (88 ABW) Public Affairs Office (PAO) and is available to the general public, including foreign nationals. Copies may be obtained from the Defense Technical Information Center (DTIC) (http://www.dtic.mil).

AFRL-RX-WP-TR-2010-4167 HAS BEEN REVIEWED AND IS APPROVED FOR PUBLICATION IN ACCORDANCE WITH THE ASSIGNED DISTRIBUTION STATEMENT.

*//Signature//   //Signature//

MARK GROFF   KENNETH A. FEESER
Program Manager   Branch Chief
Business Operations Branch   Business Operations Branch
Materials & Manufacturing Directorate   Materials & Manufacturing Directorate

This report is published in the interest of scientific and technical information exchange, and its publication does not constitute the Government's approval or disapproval of its ideas or findings.

*Disseminated copies will show "//Signature//" stamped or typed above the signature blocks.

REPORT DOCUMENTATION PAGE

Form Approved
OMB No. 0704-0188

1. REPORT DATE *(DD-MM-YY)*	2. REPORT TYPE	3. DATES COVERED *(From - To)*
March 2008	Final	04 May 2005 – 01 February 2008

4. TITLE AND SUBTITLE

COLLABORATIVE RESEARCH AND DEVELOPMENT (CR&D)

Delivery Order 0034: Aircraft Coatings Modeling and Simulation

5a. CONTRACT NUMBER
F33615-03-D-5801-0034

5b. GRANT NUMBER

5c. PROGRAM ELEMENT NUMBER
62102F

6. AUTHOR(S)

Taner Dirama

5d. PROJECT NUMBER
4349

5e. TASK NUMBER
L0

5f. WORK UNIT NUMBER
4349L0VT

7. PERFORMING ORGANIZATION NAME(S) AND ADDRESS(ES)

Universal Technology Corporation
1270 North Fairfield Road
Dayton, OH 45432-2600

8. PERFORMING ORGANIZATION REPORT NUMBER
S-531-034

9. SPONSORING/MONITORING AGENCY NAME(S) AND ADDRESS(ES)

Air Force Research Laboratory
Materials and Manufacturing Directorate
Wright-Patterson Air Force Base, OH 45433-7750
Air Force Materiel Command
United States Air Force

10. SPONSORING/MONITORING AGENCY ACRONYM(S)
AFRL/RXOB

11. SPONSORING/MONITORING AGENCY REPORT NUMBER(S)
AFRL-RX-WP-TR-2010-4167

12. DISTRIBUTION/AVAILABILITY STATEMENT

Approved for public release; distribution unlimited.

13. SUPPLEMENTARY NOTES

PAO Case Number: 88ABW-2009-0040; Clearance Date: 01 Feb 2009. Report contains color.

14. ABSTRACT

This research in support of the Air Force Research Laboratory Materials and Manufacturing Directorate was conducted at Wright-Patterson AFB, Ohio from 4 May 2005 through 1 February 2008. This task worked to develop and validate models for aircraft protective coatings in an effort to provide guidance toward novel coating materials and processes R&D. Two expectations from the effort were to establish a computational modeling capability in the surfaces and interfaces research and to transform this capability into scientific research addressing the needs of AFRL/RXBT. The former comprised of setting up of the hardware and software resources required for the technical effort. This objective was realized by acquiring workstations and multi-node clusters for the hardware requirements, and by installing relevant technical software as well as developing in-house codes for the software needs. These are listed in the software and hardware section. The latter expectation was delivered by performing research utilizing these resources in four major technical directions. These areas are: 1. Ice-phobic materials; 2. Tunable and adaptable adhesion; 3. Self-healing materials; and 4. Mechanisms of gecko adhesion.

Currently, three of these four directions are being actively investigated. Ice-phobic materials research was pursued until its early stages when the direction was changed towards adaptable adhesion. Both tunable and adaptable adhesion and self-healing materials are current areas of active research. Mechanisms of gecko adhesion is a new area that we are currently exploring.

The outcome of the work in the form of list of peer-reviewed publications and technical presentations were listed. The timeline of the technical progress was also included as compilation of the monthly reports.

15. SUBJECT TERMS

Self-assembled monolayer, arylthiol, Au(111), interface properties, Molecular dynamics simulation, binding energy, formation energy, molecular conformation, tilt angle, twist angle, dynamics, mean square displacement, molecular relaxation, polymer networks; self-healing; ionic bonds; toughness; molecular dynamics simulations, coarse-grained modeling

16. SECURITY CLASSIFICATION OF:			17. LIMITATION OF ABSTRACT:	18. NUMBER OF PAGES	19a. NAME OF RESPONSIBLE PERSON (Monitor)
a. REPORT	b. ABSTRACT	c. THIS PAGE	SAR	94	Mark Groff
Unclassified	Unclassified	Unclassified			19b. TELEPHONE NUMBER *(Include Area Code)* N/A

Standard Form 298 (Rev. 8-98)
Prescribed by ANSI Std. Z39-18

TABLE OF CONTENTS

LIST OF FIGURES

LIST OF TABLES

PUBLICATIONS AND PRESENTATIONS

Publications

1 Conformation and Dynamics of Arylthiol Self-Assembled Monolayers on Au(111). <u>Taner E. Dirama</u> and Joel A. Johnson, *Langmuir* 23(24), 12208 (2007).

2 Coarse-Grained Molecular Dynamics Simulations of Self-Healing Polymeric Networks Taner E. Dirama, Kelly L. Anderson, Joseph A. Shumaker, and Joel A. Johnson, *Mech. Time-Depend. Mater*. (submitted).

3 Probing Adhesive Interactions of Self-Assembled Monolayers of Biphenyldithiol on Au(111): Molecular Dynamics Simulation of Force-Distance Measurements in Atomic Force Microscopy. <u>Taner E. Dirama</u> and Joel A. Johnson, to be submitted to *Langmuir*.

4 Adding Self Healing Character to Polymeric Networks via Ionic Bonds: A Coarse-Grained Molecular Dynamics Simulation Study, <u>Taner E. Dirama</u> and Joel A. Johnson, SAMPE Fall Technical Conference 2007 preprint.

Presentations

1. Coarse-Grained Molecular Dynamics Simulations of Self-Healing Polymeric Networks. Apr 2, 2008, Mechanics of Time Dependent Materials Conference, Monterey, CA.

2. Conformation and Dynamics of Aromatic Self-Assembled Monolayers on Gold. Nov 8, 2007, Department of Chemical and Materials Engineering, University of Cincinnati, Cincinnati, OH. (Invited Talk).

3. Adding Self-Healing Character to Polymeric Networks via Ionic Bonds. Oct 31, 2007, SAMPE Fall Technical Conference 2007, Cincinnati, OH, USA. (Invited Talk).

4. Exploring conformations and dynamics of self-assembled thiol monolayers on Au by molecular dynamics simulations. May 23, 2007, Central Regional Meeting of the American Chemical Society, Covington, KY.

5. Molecular dynamics simulation study of conformational and dynamic properties of self-assembled thiol monolayers on Au. Mar 26, 2007, 233rd ACS National Meeting, Chicago, IL.

6. Adhesion of Ice to Surfaces. Mar 17, 2006, Nonmetallic Materials Division Technical Information Exchange on Modeling, WPAFB, OH. (Invited Talk).

1.0 HARDWARE AND SOFTWARE

1.1 Hardware

- 2 Linux Workstations (Dell)
  - <u>CPU</u>: Dual Intel Xeon 3.0 GHz (EM64T, 2 MB L2 Cache, 800 MHz Bus)
  - <u>Memory</u>: 4 GB, 400 MHz
  - <u>HD</u>: 500 GB, SATA
- Intel Fortran/C++ Compilers v 9.0, Intel Math Kernel Libraries v 8.0
- 16 node Beowulf Cluster (Western Scientific)
  - <u>CPU</u>: Dual AMD Opteron 248 2.2 GHz
  - <u>Memory</u>: 2 GB
  - <u>HD</u>: OS drive: 250 GB mirrored, RAID: 2 TB (7200 RPM SATA)
  - Interconnect: Gigabit
  - Portland Group Compiler Suite, PGI Workstation Complete

1.2 Software

- AMBER 8.0, LAMMPS
- VMD (Visual Molecular Dynamics), Mercury, SPDBV
- Ptraj (Trajectory Analysis)
- Codes developed in-house using Fortran 90, C, C++, tcl and python
  - Model building codes:
    - Dynamical cross-linking
    - SAM builder
  - Analyis codes:
    - Temperature, energies, density etc.
    - Conformational Analyis
    - Mean square displacement
    - Correlation functions
    - Scattering functions
    - Hydrogen bonding analysis
  - Visualization codes

2.0 PROJECTS

2.1 Ice-phobic Materials

The objective of this project was to bring an understanding to the adhesive interactions between coating and ice and to establish a basis of knowledge that will direct us towards the development of novel ice-phobic coatings. We approached the problem via two routes. First, we considered investigating the adhesion of ice on polyurethane, which is usually the polymer used in the topcoat. More specifically we were interested in identifying which chemical groups promote the adhesion and what types of microscopic conformation or state of the molecules on the surface make the coating more vulnerable for the ice to adhere. We also wanted to perform similar investigations on other surfaces such as silicon and teflon in order to understand the general adhesion mechanism of ice on the surfaces. Secondly, we planned on approaching the problem with an unconventional idea of understanding how nature solves it. It has been recently discovered that antifreeze proteins, found in organisms that can survive in extremely cold environments (e.g. Antarctic fish), disrupt ice growth in a non-colligative manner. These proteins may directly be utilized as ice inhibitors or the knowledge of how they function can be used for designing novel coating systems. Thus we planned on modeling the binding of ice to an antifreeze protein. This would provide insight into how the ice formation problem is solved in nature which in turn will provide clues as to how this problem may be solved via synthetic methods. Therefore, how they function could be used to design biomimetic coating systems with inherent anti-icing capability.

2.1.1 Modeling ice crystal

We started with reviewing the literature on the modeling of ice surface and analyzed various types of crystal forms of ice. It was feasible to model ice 1h, which is the most energetically favorable form. Besides the positions of the oxygen atoms that has to satisfy the experimentally determined unit cell for ice 1h, the positions of the hydrogen atoms is also important. Namely, there is randomness in the hydrogen bonding. This randomness has to satisfy the "ice rules" determined by Bernal and Fowler. Additionally, the unit cell has to have zero net dipole moment and minimal net quadrupole moment. I implemented the results of a work by Hayward and Reimers so that all these requirements are met without having to go through time consuming Monte Carlo simulation to create the unit cells. This implementation is realized by a

Fortran code I developed using GNU Fortran77. The resulting unit cells can directly be used for any future modeling studies that involve ice 1h.

Figure 1. (Left) Ice 1h. (Right) An anti-freeze protein.

2.1.2   Modeling of polyurethane resin

Polyurethane (the main constituent in topcoat of an aircraft paint) slab was modeled in order to create the surface on which the ice will adhere and the adhesive interactions of will be studied. The molecule used in the modeling is a dimer of a product of the reaction of m-Phenylene diisocyanate with ethylene glycol. This molecule has been chosen for its simplicity in order to evaluate the success of the force field and the simulation protocol. While AMBER molecular dynamics program package has shown that it is capable of modeling and simulating the amorphous polyurethane system at the realistic density successfully, it lacks some features that enable conveniently modeling of a two phase system such as ice and polyurethane. Therefore, we intended incorporating LAMMPS molecular modeling package for modeling the interface. Thereore, codes needed to be developed for the following purposes. First codes that make AMBER coordinate and topology files portable to LAMMPS environment and vice versa. Then programs that analyze output from LAMMPS simulations and calculate averages and standard deviations for several quantities and plot the results in graphs automatically.

Next step was to model an isocyanurate molecule and an oligomer of polyester polyol. The crosslinking reactions of the two molecules produce crosslinked polyurethane; the type that is commonly used in aircraft topcoats. Then FORTRAN code that creates a simulation box of binary blends on a cubical lattice was developed. Using this initial configuration created by this

3

program we have performed equilibration simulations of isocyanurate and polyester. Using this equilibrated structure I have built another simulation box of the topcoat (isocyanurate and polyester) and the ice crystal. This initial configuration was further equilibrated and the ice-topcoat interface was obtained. Next, we began working on calculating the energy of adhesion.

For the purpose of making crosslinked polyurethane thus modeling of a more realistic coating system, I have also been working on the modeling the crosslinking reaction. As reactions are not supported by simulation software, it was necessary for me to develop a programming code that performs this task. We completed developing the crosslinking code "xlinker". The resulting over 1300 line long code will likely be an important tool for creating crosslinked coating systems towards the modeling and simulation efforts in the paints and coatings group. The main function of the code is to determine the candidate reacting pairs and carry out the reactions. In doing this it sorts the reacting pairs with respect to their closeness thus closer pairs are given priority in the order of reaction. From the modeling point of view, the reaction of a pair of reacting groups mean that a set of changes occur on several atoms in the reacting molecules. These modifications include change of atom types, bond types, angle types and dihedral angle types. Additionally, some existing bonds, angles and dihedrals removed and new ones created.

An important feature of the code is that it performs crosslinking reaction of molecules in the primary simulation box with their images. Therefore, one can build crosslinked molecules with infinite length in any of the three dimensions. The modeled system therefore becomes very similar to the real systems. Figure (a) shows a two dimensional projection of a crosslinked molecule that is infinite in x and y directions.

The crosslinked system needs to be characterized in order to know the micro-scale architecture of the crosslinked molecules. The code performs a complete analysis and reports a wide set of information including density of crosslinking reactions, percentage of reactions, number of newly formed chains and their size, the members of newly formed chains, which reactive group in which molecules is linked with which other groups etc.

Figure 2. (Left) Repeating group in polyurethane resin and the ice polyurethane interface. (Right) Two dimensional view of cross-linked polyurethane molecule.

2.2   Tunable and Adaptable Adhesion

2.2.1   Conformation and Dynamics of Self-Assembled Monolayers

Introduction

Self-assembled monolayers (SAMs) of alkanethiols provide many unique features that make them attractive to various applications, including electrochemical sensors[1,2], biosensors[3], patterning of surfaces[4], friction and lubrication control[5], protective coatings[6], and molecular electronics[7]. Foremost, they are relatively easily formed through solution or gas phase deposition and form a highly ordered and densely packed monolayer. Thiol groups chemisorb or physisorb onto surfaces of Au, Ag and Cu; both experimental and theoretical evidence has proven that sulfur atoms coordinate strongly to a Au surface.[8,9]. Another important feature of SAMs is their tunability. The surface properties can easily be tailored by alternative tail groups or chain lengths as a tuning parameter. For instance, the selection of short-chain alkanethiols provide a pathway for electrochemical reactions to take place on the metal surface in sensor applications, while long-chain alkanethiols enable blocking of the metal substrate in applications such as corrosion protection.[2] Yet, perhaps the most appealing feature of SAMs is that they provide a molecular level control over the surfaces they are applied on.

The attractive features of SAMs have induced significant attention that resulted in a wealth of studies addressing the preparation, the characterization, and the application aspects as summarized in comprehensive reviews.[2,10-14] Yet, there remain some essential questions to be fully answered, such as: what are the parameters that control the growth and the structure, and

what are the driving forces that render the monolayer stable or otherwise? Understanding such questions will clarify the mechanisms involved in the growth and the structure in SAMs, which in turn will help designing better and more targeted SAMs.[11] In addition, a thorough characterization of the precise geometry and the structure of SAMs is critical from a technological point of view, particularly in molecular electronics applications where the molecular orientation has direct consequences on current-voltage relationship.[15-17] Evidently, good control over the molecule-substrate interface is crucial in such applications. Controlling the interface is not only a static matter, the dynamics is also involved which is an overlooked topic as compared to other subjects.

SAM structures are commonly created using aliphatic and aromatic alkanethiols. Aromatic thiols differ from linear thiols in that they are generally more rigid and they entail stronger molecule-molecule interactions. Additionally, the tunability is relatively easily facilitated by aromatic thiols since the protons around the phenyl rings can readily be substituted with various chemical groups to target certain properties. Nevertheless, relatively fewer experimental and theoretical studies focused on understanding the system geometry of SAMs of aromatic alkanethiols, while a substantial extent of such effort was devoted to aliphatic alkanethiols. In one of such studies Jung *et al.*[18] performed MD simulations of SAMs of aromatic thiols to investigate the ordering and the conformational behavior. Their model involved the assumption of a deprotonated thiol group forming a covalent bond at the 3-fold hollow site on a Au(111) surface. The bond formed between the sulfur head group and three Au atoms were modeled using a harmonic potential. Therefore, the sulfur atom was in effect anchored to the 3-fold hollow site and it was virtually impossible to observe it visiting another site on Au(111). On the contrary, Kim *et al.*[19] have adapted a non-bonded potential to account for Au-biphenyldithiol (BPDT) interactions. The resulting binding energy for the chemisorption was in reasonable agreement with experimental measurements. Moreover, their force field simulations for the S-Au distance as well as the tilt angle showed a good agreement with their complementary Density Functional Theory (DFT) calculations.

Establishing the gold-thiol interaction with a non-bonded potential releases the restriction on the thiol molecule so that it is allowed to hop from one site to another; thus, provides a closer representation to the *true dynamics* of the organothiols. In fact, the mobility of the adsorbed thiol on Au surfaces has been demonstrated experimentally.[20-23] For instance, when a linear

alkanethiol SAM was placed in a solution of aromatic alkanethiols, the substitution of the linear alkanethiols was observed at the domain boundaries; implying that the S-Au bond breaks without an external impulse.[22] More recent evidence to the mobility was the observation that the stochastic on-off conductivity switching, formerly demonstrated in phenylene-ethylene oligomers, exists also with very simple SAMs of alkanedithiols on Au(111) surface.[23] This finding suggested also that the bond between the thiol and Au breaks quite frequently leading to on-off mechanism.

Our goal in this effort was to characterize the conformational and the dynamical properties of arylthiol SAMs and to contribute to the understanding of the influence of chemical structure on such properties. With this purpose in mind, we selected six arylthiols: 1,4-benzenedimethanethiol (BDMT), benzylmercaptan (BM), biphenyldithiol (BPDT), thiophenol (TP), 4-methylbenzenethiol (TT) and 4-methylbenzylthiol (XT) (see Figure 3). SAMs of all six and similar arylthiols with a single or two phenyl groups in standing up configuration were formed earlier and some experimental and theoretical data were available.[17-19, 24-28] We followed a similar approach to the work of Kim *et al.*[19] to account for Au-thiol interactions by representing them using a non-bonded potential.

Model

We used General Amber Force Field (GAFF)[29] to describe the intramolecular and intermolecular interactions of arylthiol molecules. GAFF is an extension to Amber force field, which was designed specifically for amino acids and nucleic acids, to cover general organic species. The performance of GAFF parameters has been successfully tested in terms of crystalline state conformations, conformational energies and dynamical properties for various small organic molecules.[29, 30] In addition, we performed bulk simulation of BDMT and TP. The bulk density was within 3% of the experimental data. Au-Au interactions were neglected by excluding them from the neighbor list and Au atoms were held steady by setting the force imposed by organic molecules to zero. Keeping the Au atoms effectively frozen was justified by the work of Kim et al.[19] who investigated the effect of Au relaxation on conformations of SAMs of BPDT. They found that Au relaxation has a negligible effect on the SAM conformations. The intermolecular interactions between self-assembling molecules and Au atoms were described by the Dreiding Force Field (FF)[31] with optimized parameters.[32] To describe these non-bonded van der Walls interactions, we used an exponential-6 form.

$$E_{ij} = D\left[\left(\frac{6}{\zeta-6}\right)\exp\left(\zeta\left(1-\frac{R_{ij}}{R}\right)\right) - \left(\frac{\zeta}{\zeta-6}\right)\left(\frac{R_{ij}}{R}\right)^{-6}\right] \qquad (1)$$

Here, D is the depth of the energy well, R_{ij} is the distance between atoms, R is the distance at energy minimum and ζ is a dimensionless constant, were the default value of $\zeta = 12$ was used.

Dreiding force field (FF) parameters were optimized by Jang *et al.*[32] using DFT targeting the interactions between Au atoms and those in the molecules. Briefly, they used ethanethiol as a model organothiol on a $Au_{32}(111)$ cluster with S initially positioned at FCC and HCP sites (see Figure 4). The resulting net binding energy of 24.53 kcal/mol for the most stable FCC site compares reasonably well with the experimental value of 30.11 kcal/mol.[33] Subsequently, the optimized geometry and DFT calculated binding energies were used in fitting the FF parameters for the Au-S interaction. The non-bonded interaction parameters between Au and other atoms in organothiols were obtained by geometric mean of the Au parameter in Universal FF[34] and the other atoms from Dreiding FF[31]. We used these parameters directly for our model (see Table 1).

Our selection of GAFF force field for taking into account the organic interactions while using Dreiding FF for the organic-Au interactions stem mainly from GAFF being a more comprehensive force field than Dreiding FF. Therefore, the various atom types in self assembling molecules can effectively be represented while the accurate representation of the improved Dreiding FF of the organic-Au interactions is facilitated. In order to verify this approach we calculated some conformational properties of SAMs of three linear alkanethiols: $C_{10}SH$, $C_{18}SH$ and $C_{30}SH$ that are modeled and simulated using the same method as in this work.[35] The tilting angles were estimated within 2° of the Grazing Incidence X-ray Diffraction (GIXD) measurements.[36] While the tilt direction estimates were not as accurate (they differed as much as 9°), they showed qualitative agreement with the experimental findings on the chain length dependency. In addition, we attempted estimating the melting temperature of the SAM of $C_{10}SH$. For this purpose, we performed simulations in which the SAM was gradually heated. Our resulting estimate of $T_m=110\ ^o C$ agreed reasonably well with GIXD results of $T_m =\sim100\ ^o C$.[11]

In order to construct the Au(111) slab, an FCC lattice with a lattice spacing of 4.0782 Å was created and the 111 plane was oriented along the z-axis. The resulting Au(111) slab consisted of a total of 4860 atoms arranged in $27 \times 30 \times 6$ in x, y and z-directions.

The arylthiol molecules were built using the LEAP module in AMBER[37]. Point charges on atoms were calculated using the AM1-BCC method[38] which was parameterized to reproduce HF/6-31G* RESP charges. Experimental findings suggest, on an ideal surface of Au(111), that self-assembling organothiols arrange on a ($\sqrt{3}\times\sqrt{3}$)-$R30°$ triangular lattice while S atoms are positioned on the FCC (i.e. 3-fold hollow) site.[39] A monolayer was formed by accordingly placing 270 organothiol molecules. The conformation of a self-assembling molecule with respect to the substrate is defined by three angles: the tilt angle (θ), the azimuthal angle (ϕ) and the twist angle (ψ) (see Figure 5). The orientation of each self-assembling molecule was initially set to standing up position by setting $\theta = 0$, $\phi = 90$ and $\psi = 0$. Afterward they were randomly rotated around the z-axis giving a random value to each ψ. A 2-dimensional view to a randomly oriented initial SAM structure is shown in Figure 6 Figure 6 (a). The dimensions of the simulation box were set to be 77.86, 74.92 and 200.00 Å in x, y and z directions, respectively. Setting a very large box dimension in the z-direction rendered true 3-dimensional periodic boundary conditions as effectively 2-dimensional.

Simulation Protocol

The MD simulations were performed using LAMMPS (Large-scale Atomic/Molecular Massively Parallel Simulator).[40] Lennard-Jones and Coulombic interactions for pairs of organic atoms were computed using a switching function with inner and outer cutoffs of 14 and 16 Å, respectively, whereas the cutoff for the interactions of Au-organic atom pairs was set to be 14 Å. The long range Coulombic interactions beyond the cutoff (reciprocal sum) were calculated using the particle-particle particle-mesh Ewald (PPPM) solver[41] with a precision value of 1.0×10^{-4}. The equations of motion were integrated using the Verlet algorithm[42] with a time step of 1 fs. The SHAKE algorithm was applied to all hydrogen atoms. Temperature in a canonical (NVT) ensemble was controlled using the Nosé/Hoover thermostat.[43, 44]

The system was minimized using a conjugate gradient algorithm followed by gradually raising the temperature from 0 to 900 K where it was equilibrated for 400 ps in the NVT ensemble. At this stage of the equilibration, the sulfur atoms on the Au(111) surface were fixed. Following a gradual cooling to 300 K, the system was further equilibrated after removing the

constraints imposed on the S atoms for 50 ps and 100 ps in NVT and NVE ensembles, respectively. A 3-dimensional view of the *xz-* (upper) and *yz-* (lower) planes for the equilibrated SAM of BPDT is shown in Figure 6 (b). Subsequent to the equilibration, the trajectories were produced in NVE and saved for later analysis for the first 5 ps and then 500 ps with 0.001 ps and 0.1 ps increments, respectively. While the most of the calculations were made based on the simulations of 500 ps, we ran an additional much longer simulation of 10 ns only for TT.

Results

To characterize the conformations of arylthiols the probability distribution functions for the tilt, twist and azimuthal angles were calculated and are presented in Figures 5 through 7. The peak positions for ϕ and ψ were obtained by Gaussian function fits, whereas for θ either Gaussian or asymmetric double sigmoidal functions were used, depending on the shape of the distribution function. The results for the peak position as well as the full width at half maximum (FWHM) were tabulated and presented in Table 2.

BPDT shows the narrowest distribution of θ with its peak at 13.0^o (see Figure 7). A tilt angle of 13.2^o reported by Kim, *et al.*[19] using DFT is in excellent agreement with our model. Their model based on MD simulation, on the other hand, yielded a somewhat higher value of 18.4^o. BDMT and BM have broader distributions with peaks around 8°. TP and TT have double peaks: the first peaks are around 11° and the second peaks are at 41° and 31°, respectively. In order to quantify the relative weight of each peak, we fitted asymmetric double sigmoidal and Gaussian functions for the former and the latter, respectively. The subsequent integration of these functions showed that the dominant peak at low angles comprise 70% and 85% of the overall distribution for TP and TT, respectively. Thus, in both cases only a small portion of the self-assembling molecules tilt at a higher degree. We explain the possible origins of the second peak below.

The experimental data of the tilting angle of the SAMs is commonly obtained from the analysis of the q_z-dependence of the grazing incidence X-ray diffraction (GIXD) intensity. GIXD measurements of 4-methyl-4'-mercaptobiphenyl indicated an upper limit of 19° for the tilt angle, which is substantially smaller than ~30° for *n*-alkane thiols.[45] Hence, our simulation results are within the boundary provided by this experimental measurement. It is worthy to note that the lower tilting angles associated with arylthiols suggest that the van der Waals dimensions for the

arylthiol molecule are large enough to fill the area available for each molecule on the ($\sqrt{3}\times\sqrt{3}$)-$R30°$ lattice structure by tilting at a smaller degree than those of n-alkane thiols.[11]

In Figure 8 the azimuthal angle (ϕ) does not show any appreciable deviation from the initial configuration, even though the distributions are rather dissimilar. Resembling the case of θ, the BPDT has a very narrow distribution while TP has the broadest distribution of all. By looking into the behavior of ψ, in Figure 9 we observe that there are two distinct and alike peaks as expected from a herringbone conformation for all molecules except TP. The first and the second peaks are located (on average) at 53° and 127 ^{o}. These peaks, on the other hand, are shifted to 64° and 115° for TP. TP has two additional peaks appearing at the low and high end of the distribution scale, specifically at 4° and 176°.

The MD simulation study by Jung, et $al.$[18] investigated the conformational behavior of BM and TP that were anchored on Au(111) each by a thiolate bond with ($\sqrt{3}\times\sqrt{3}$)-$R30°$ unit cell arrangement. It is interesting to note that while their model was constructed in a fundamentally different approach than this work, many of the conformational properties agree. For instance, both BM and TP were found to form a herringbone structure, with the latter having a less defined arrangement. They found that TP formed four ψ peaks at 15, 65, 116 and 174° as compared to our findings of 4, 64, 115 and 176°. Moreover, the tilt angle for BM was 9° versus our estimate of 8°. However, their tilt angle for TP was 25°, which is in the range of n-alkanethiols, versus our estimate of 12°.

TP differs from the other molecules not only with its different number of peaks in ψ but also with the broad distribution over the angle scale. Even the minima regions are comprised of appreciable populations of conformations indicating that TP does not have a well-defined herringbone conformation. In order to understand the origins behind the four-peak-distribution we need to investigate the two-dimensional ordering in Figure 6 (c), more closely. It appears that, unlike in SAMs of BPDT (Figure 6(b)) and the other molecules, TP has heterogeneous herringbone structure formation with three-directional orientation. The first direction along the vertical axis has the same orientation as in BPDT. The other two directions are rotated by +60° and −60° with respect to the vertical axis. Therefore, there is a boundary region separating these smaller conformationally unalike domains. In fact, the secondary peak observed at higher values of θ in TP could be a result of the anomalies at this boundary region.

Another focus of our interest was to examine the Au(111) sites (i.e. FCC, HCP, *Bridge* and *Top*) that the thiol head groups favor. With this purpose in mind, we determined the Au(111) surface sites at which the sulfur atom is positioned at each time step of the simulation. The criteria used to determine the sulfur position on the Au(111) surface sites was as follows. If a sulfur atom was within 0.42 Å (i.e. ¼ of the distance between FCC and HCP sites) of a site then the sulfur was assigned to that site. The cases in which the sulfur position was outside of a 0.42 Å limit of any site were neglected. Such occurrences comprised less than 0.1% of all. Table 3 presents the fraction of occurrences for each site over all 270 molecules and 5000 steps of a 500 ps-long simulation. It is clear that FCC is the dominant site for all molecules. The *Bridge* site is rarely (1-2%) occupied by any of the self-assembling molecules. HCP, on the other hand, has a wide range of preference from 0 to 40%. The most peculiar behaviors of the site preference are observed in BPDT and TP. BPDT goes almost exclusively to the FCC site and it almost never visits either an HCP or a *Bridge* site. Interestingly, TP visits FCC and HCP sites nearly equally. The occurrence of the *Top* site was inexistent.

In order to put these results into the perspective of thermodynamics, we reviewed previous theoretical studies. DFT calculations of single n-*alkane* thiols on a Au(111) surface were performed in order to understand the energy levels involved in positioning of S on the Au sites.[46] For a single CH_3S, the FCC site was found to be the lowest energy state followed by HCP by an energy cost of 0.10 eV. *Bridge* and *Top* positions were local energy maxima with costs of 0.40 and 0.95 eV, respectively. Other thiols with a higher number of alkane groups were found to follow the same trend confirming that FCC site is the most stable among all four sites on Au(111). The above analysis of site positioning had shown that this order of energy levels corresponding to lattice sites is the major mechanism for the SAMs of arylthiols. Namely, FCC is clearly the most visited site followed by HCP. *Bridge* site was visited dramatically less frequently than HCP which represents characteristics of an energy maximum. A substantially higher energy penalty associated with the *Top* site makes its occurrence so rare that through the course of our simulation it has never been observed. We revisit the site positioning issue in the discussion section.

The distance between S and Au atoms is a critical parameter in SAMs that we can use to compare our results from higher level theories. Average distances (d_{Au-S}) between S atoms on the Au(111) surface and its three nearest Au atoms are presented in Table 4. The distances at each

time step (every 0.1 ps) were first averaged over the number of sulfur atoms followed by averaging over the number of time steps. Standard deviations obtained from the second averaging process were presented as means of error. d_{Au-S} for BPDT from DFT calculations was reported as 2.64 Å by Kim, *et al.*.[19] This result is in excellent agreement with our modeling estimate of 2.66 Å. When the sulfur atoms were binned with respect to their positions on the Au(111) surface sites, the order of d_{Au-S} was obtained for all molecules consistently as FCC < HCP < *Bridge*. This order follows the intuition due to the energy levels of the sites mentioned above. Explicitly, the lower the energy state, the closer the Au-S pair is. The variations of d_{Au-S} among the molecules are minimal; in fact, within the errors.

The formation of SAMs is driven by the strong interactions between the head groups and the metal substrate as well the inter-chain interactions among self-assembling molecules. The resulting structure comes about due the interplay between the two interactions types. These interactions are commonly described by the binding energy (E_b) and the SAM formation energy (E_f). We define E_b and E_f in equations 2 and 3, respectively, where $E_{vdW,all}$ refers to the total van der Waals energy of the SAM-Au system, $E_{vdW,mol}$ is the van der Waals energy of molecule-molecule interactions, E_{pot}, is the potential energy of the SAM-Au system, E_{gas} is the potential energy of a molecule in the gas phase and n stands for the number of self-assembling molecules.

$$E_b = \frac{E_{vdW,all} - E_{vdW,mol}}{n} \qquad (2)$$

$$E_f = \frac{E_{pot} - n \times E_{gas}}{n} \qquad (3)$$

E_b ranges between 25 and 26 kcal/mol for the arylthiols (Table 5). Apparently, it does not show any conclusive variation among the molecules. Thus, the molecular structure does not significantly affect E_b. The value of E_b shows a good agreement with that of ethanethiol on Au(111) obtained by DFT calculations, 24.53 kcal/mol.[32] The experimental results for various organothiols measured by helium beam reflectivity and temperature-programmed desorption also showed that the backbone has little effect on E_b, which ranged from 29.6 to 31.8 kcal/mol.[33] Our modeling results are in reasonable agreement with these experimental measurements. E_f shows, on the contrary, a considerable variation with chemical structure. Obviously, the molecular structure has a noticeable effect on the molecule-molecule interactions which lead to substantial variations in E_f. The order of the magnitudes for E_f is BPDT > BDMT > XT > BM > TT > TP.

13

While our previous analysis of the sulfur sites (see Table 3) showed the probability of finding self-assembling molecules at a specific site and a given time, it did not provide information about the dynamics of the site positioning. In order to shed some light on the dynamics aspect, we performed a correlation function analysis. Accordingly, the correlation function was defined by the following equation:

$$c_i(t) = \frac{\langle p_i(t+t_0)p_i(t_0) \rangle}{\langle p_i(t) \rangle} \qquad (4)$$

where $p_i(t)$ is *the site position population operator*, which is equal to 1 when a sulfur atom is positioned at the site i (e.g. i = FCC, HCP or *Bridge*) at time t, and 0 otherwise. Thus, $c_i(t)$ describes the probability that a sulfur atom originally positioned at site i at $t= t_0$ stays at the same site at time $t= t_0+t$. The brackets represent averaging over S atoms and reference time. While we used the trajectory of 500 ps long in the calculations, we will present the data only up to 100 ps taking into account the statistical error in time correlation functions. The resulting time correlation functions for BM at the three observable sites were presented in Figure 10. $c(t)$ for the *Bridge* site decays very rapidly. FCC site is the most stable of the three: less than 80% of $c(t)$ decayed in 100 ps. HCP site has an intermediate level of stability with about 50% of decay in $c(t)$.

$c(t)$ for each arylthiol were compared in Figure 11 in order to characterize the relative stabilities of the S head groups at the three sites. The first observation to notice is that the relaxation is not a first order process. An initial relaxation occurs around 0.1 ps and at longer times a second process comes into play. Hence, a second order exponential decay can be a good model for fitting $c(t)$. Indeed, we obtained the lifetime of relaxations for HCP and *Bridge* sites from the second order exponential fits as presented in Table 6. We did not obtain the lifetimes for FCC site due to the lack of decay in the correlation functions for a plausible extrapolation of the fitting within the accessible time scale.

BPDT clearly shows the highest level of FCC site stability. In fact, in this scale its second relaxation process is imperceptible. TP, on the other hand, has the fastest decay, indicating that it has the shortest tendency to stay at FCC site followed by TT. XT and BDM have nearly the same intermediate levels of stability towards the FCC site. By evaluating the HCP site stability in Figure 11 (b) we observe that the trend nearly reverses; the lifetimes (see Table 6) show that the

14

order of stability is TP > BM > XT > TT > BDMT > BPDT. There is a significant difference between the longest and the shortest lifetimes; 551 vs. 9 ps. In contrast to the two other sites, the relative variations in decaying of $c(t)$ for different molecules are not present for the *Bridge* site: the lifetimes range within $7\text{-}8 \times 10^{-2}$ ps. In order to elaborate on the nature of the *Bridge* site, we generated a plot that traces the trajectory of a TP head group. TP was selected for its relatively higher mobility than other molecules as well as its nearly equivalent tendency in being either at FCC and HCP sites. It is clear in Figure 12, where multiple hopping is observed, that the head group spends the majority of time at either FCC or HCP locations with *Bridge* sites visited momentarily during the hopping from one to the other minima. It appears that the sulfur atoms are found to be at *Bridge* site because of the fact that it lies on the path between two minima (i.e. *FCC* and *HCP*). Therefore, *Bridge* site exhibits characteristics of a *local* energy maximum along the pathway between *FCC* and *HCP* sites. Note also that the *Top* position and its surrounding area, as indicated previously, have never been visited. This observation is an indication that the *Top* site is the *global* maximum on the surface. The DFT calculations of methanethiol and ethanethiol support these conclusions.[46]

The dynamics of SAMs were characterized using a weight averaged mean square displacement ($\langle u^2 \rangle$), in which $\langle u^2 \rangle$ was derived as a function of time from the MD trajectories through the relationship:

$$\langle u^2 \rangle(t) = \left\langle \left(r(t+t_0) - r(t_0) \right)^2 \right\rangle \qquad (5)$$

where $r(t_0)$ and $r(t+t_0)$ are the coordinates of atoms at reference time t_0 and after time t. Brackets represent averaging over atoms and reference time. $\langle u^2 \rangle$ was obtained after averaging over 500 ps using multiple time origins.

Until about 2 ps, all arylthiols exhibit similar dynamical behaviors as seen in Figure 13. This is the time scale that corresponds to the relaxation times for the vibrational and the rotational motions of small side groups such as thiol, methyl and methyl-thiol, or rotations of phenyl groups around their equilibrium configurations. Since the molecular structures of the self-assembling molecules are fairly similar, it is expected that such vibrational and rotational motions are alike. However, above the 2 ps time scale, $\langle u^2 \rangle$ exhibits entirely different behavior. For instance, $\langle u^2 \rangle$ reaches a plateau for BPDT within a few ps, while TP shows no sign of

leveling off within the scale of the plot (i.e., 100 ps). Apparently, there is a very rich and distinct dynamical behavior at $t > 2$ ps for molecules of similar chemical structures.

Discussion

We observed unique dynamical behaviors of SAMs after analyzing $\langle u^2 \rangle$, particularly in the longer time scale region of Figure 13. For instance, $\langle u^2 \rangle$ for TP continues to rise at long times, whereas in the case of BPDT there is an extended plateau. Understanding the origins of this observation requires a careful analysis of the different motions that contribute to the overall dynamics of SAMs. When examining the relaxation of the HCP sites, we notice that BPDT relaxes with a lifetime of 9 ps (see Table 6). It would be expected that this relaxation presents itself in $\langle u^2 \rangle$, perhaps as a plateau. However, the HCP-relaxation merges together with the vibrational and the rotational contributions that occur in the same time scale, resulting in an absence of a separate plateau at this short time scale. On the other hand, TP has an HCP-relaxation of 551 ps, which naturally does not present itself in this time scale; instead of a leveling off, $\langle u^2 \rangle$ continues to rise. BDMT is the second molecule after BPDT that shows the shortest HCP-relaxation with $\tau = 73$ ps. Note that the corresponding plateau to this relaxation is also observed.

In order to elucidate this emerging relationship between the relaxation of the sulfur at the Au(111) sites and the overall dynamics of SAMs, we plotted overlaid graphs of $\langle u^2 \rangle(t)$ and $c(t)$ in Figure 14 using TT as an exemplar molecule. Note that, in this particular case, we present the data extending over a much longer time scales (10^{-2} ps $< t < 5 \times 10^3$ ps). The time at which a single exponential function decays to 0.368 (i.e. e^{-1}) is its lifetime. Therefore, we used this number (horizontal dashed line) as guidance to the point t where $c(t)$ has decayed and reached its lifetime, approximately. Taking the HCP site into account, it can clearly be seen that when $c(t)$ intersects with the horizontal dashed line $\langle u^2 \rangle(t)$ exhibits a leveling off. The reason for the leveling off is because prior to the relaxation time for HCP site had been reached, the HCP site relaxation was occurring that was giving rise to $\langle u^2 \rangle(t)$. Subsequent to the completion of the substantial relaxation, the HCP site relaxation no longer affects dynamics notably. At later times, $\langle u^2 \rangle(t)$ shows a rapid increase due to the fact that the FCC relaxation has not fully taken place in that time scale. Since we are bounded by the length of the simulation we can practically achieve,

we are unable to observe the complete decay of $c(t)$ for FCC. However, at much longer time scales when FCC exhibits a complete decay, we would expect to recognize a corresponding plateau in $\langle u^2 \rangle(t)$. Identifying the influence of the *Bridge* site decay, on the other hand, is complicated by the co-occurrence of other modes of motion (i.e., vibrational and rotational). Moreover, the relaxation of this site contributes to the overall dynamics very minimally, since there is a small number of thiol groups positioned at this site at a time.

The above analysis shows that the hopping of the sulfur head group from one site to another results in a significant amount of translational motion in the entire molecule and that overall the dynamics of SAMs at the picosecond-nanosecond time scale is driven by this motion. On the other hand, if the sulfur atom were to be fixed at a particular site as in many of the previous MD simulations studies, the motion of the molecule would stem mainly from the rotational and vibrational sources leading most likely to indifferent dynamics of SAMs. Therefore, it is an important note of clarity that the results for the unique dynamical behavior accrue from our model that treats the sulfur-Au interaction as non-bonded. We discussed previously in Sec. I the experimental evidence supporting the treatment of sulfur-Au interaction via a non-bonded potential. In addition, we present below indirect verification of this treatment in capturing proper structural and dynamical properties of actual SAMs.

One key objective of this work was to relate some of the modeling results to experimentally measured properties of actual SAMs. First, the degree of order that we assess by the angle distributions and the site positioning can be compared against the experimental measurements. Dhirani et al.[47] studied the degree of order in SAMs of oligo(phenylethynyl)benzenethiols with 1, 2 and 3 phenyl rings using scanning tunneling microscopy (STM). They found that the degree of order increases with the number of phenyl groups. Our finding that the arylthiol with two phenyl groups (i.e. BPDT) is more stable than the rest of the arylthiols with a single phenyl group is supported with this finding. Secondly, we compare the degree of integrity, in some respects the stability, of SAMs as characterized by the surface coverage to our data. Pugmire et al.[28] prepared SAMs of all arylthiols modeled in this work except BPDT from solution or vapor on Au substrate. They reported the surface coverages (i.e., the degree of integrity) of these SAMs as measured by X-ray Photoelectron Spectroscopy (XPS). The order of the surface coverages for the SAMs from the highest to the lowest was BDMT, XT, BM, TT and TP. It is quite interesting to note that our results of a simple and

idealized model for E_f followed the same order (see Table 5) with the degree of integrity of the actual samples containing a variety of defects and impurities. This probable correlation suggests that the SAM formation energy is an important parameter that has implications on the structure of SAMs. This inference was supported also by Gooding *et al.*[2] who pointed to the positive correlation between the molecule-molecule interactions and the thermal stability.

We may draw attention also to the correlation between the FCC site stability and the surface coverage. When all the thiol groups are at the lowest energy state of FCC site, they can collectively facilitate the molecule-molecule interaction energy. This type of ordering will bring about a cohesive monolayer that will likely translate into a higher surface coverage. On the other hand, consider a single thiol group visiting a higher energy site (e.g. HCP and *Bridge*) with all its neighbors are at the FCC site. Its new position will raise the energy of the SAM not only because of being at a higher energy lattice site, but also because it will inflict the neighboring molecules to rearrange their conformations due to closer contact. As this type of visits become more frequent the cohesive nature of the SAM will diminish leading perhaps to a lesser degree of integrity. We argue that this scenario not only links the FCC site stability estimates of our idealized model to the surface coverages of actual SAMs; but also it is possibly the mechanism relating dynamics to structure.

Summary

We predicted the conformational and the dynamical properties of SAMs for a series of arylthiols on a Au(111) surface using MD simulations. The results of arylthiol configurations showed a good agreement with DFT calculations as well as experiments. Treating Au-thiol interactions using a strong non-bonded interaction potential enabled the thiol groups to visit other sites besides FCC. BPDT was found to form the most well-defined herringbone structure with thiol head groups positioned predominantly at the energetically favored FCC site. The stability of the head groups at each Au site was characterized by time-dependent correlation functions. They revealed that the FCC site has the longest relaxation time followed by the HCP site, while the Bridge site showed characteristics of a local energy maximum. Moreover, these site dynamics exhibited a direct correspondence to the overall dynamical behaviors of arylthiols. Coupled with our observation that there is a correlation between the SAM formation energy (Ef) and the FCC site stability, we inferred that Ef is a crucial parameter that controls the structural and dynamical behaviors of SAMs.

Tables

Table 1. Dreiding FF parameters employed for non-bonded interactions between atoms of organic molecules and Au atoms from Jang *et al.*[32]

Pair	D *(kcal/mol)*	R *(Å)*
Au-S	9.033	2.682
Au-C	0.064	3.561
Au-H	0.041	3.082

Table 2. Peak positions and FWHM values of angle probability distribution functions.

			BDMT	*BM*	*BPDT*	*TP*	*TT*	*XT*
θ	G or A*		A	A	G	A	G	G
	1st peak	peak position	8.2	8.0	13.0	11.6	10.9	12.3
		FWHM	9.9	11.9	6.1	15.5	12.2	9.3
ϕ	1st peak	peak position	0.8	-0.5	-1.5	1.5	9.8	1.5
		FWHM	25.1	25.3	7.7	26.7	15.3	14.1
ψ	1st peak	peak position	52.6	53.3	52.5	64. 2	53.1	53.2
		FWHM	18.2	22.5	20.4	26.2	23.5	20.1
	2nd peak	peak position	127.5	127.0	127.5	114.9	127.2	127.0
		FWHM	18.0	22.3	20.3	24.0	24.0	20.1

* G and A refers to the fitting function used. G: Gaussian, A: Asymmetric double sigmoid function.

Table 3. Fraction of S atoms positioned at the three Au(111) lattice sites.

	FCC	HCP	*Bridge*
BDMT	0.93	0.05	0.01
BM	0.82	0.16	0.02
BPDT	0.98	0.00	0.01
TP	0.49	0.40	0.02
TT	0.78	0.19	0.02
XT	0.84	0.14	0.02

Table 4. Average distance ($d_{Au\text{-}S}$) between S atoms on the Au(111) surface and their nearest three Au atoms in Å.

Site	BDMT	BM	BPDT	TP	TT	XT
FCC	2.660 ± 0.003	2.661 ± 0.004	2.661 ± 0.003	2.667 ± 0.005	2.663 ± 0.004	2.662 ± 0.003
HCP	2.709 ± 0.028	2.668 ± 0.017	2.688 ± 0.081	2.682 ± 0.006	2.695 ± 0.012	2.689 ± 0.020
Bridge	2.712 ± 0.049	2.721 ± 0.047	2.757 ± 0.037	2.744 ± 0.034	2.766 ± 0.029	2.719 ± 0.044
all	2.663 ± 0.003	2.668 ± 0.006	2.663 ± 0.003	2.683 ± 0.004	2.674 ± 0.004	2.667 ± 0.005

Table 5. Binding (E_b) and formation (E_f) energies in kcal/mol.

E (kcal/mol)	BDMT	BM	BPDT	TP	TT	XT
E_b	-25.8	-25.3	-25.1	-25.2	-25.3	-25.7
E_f	-70.4	-67.1	-81.6	-61.4	-64.2	-68.1

Table 6. Lifetime (in ps) of sulfur atom positions at the HCP and *Bridge* sites.

	BDMT	BM	BPDT	TP	TT	XT
HCP[†]	73	219	9	551	190	216
Bridge[‡]	8×10^{-2}	7×10^{-2}	7×10^{-2}	8×10^{-2}	7×10^{-2}	7×10^{-2}

[†] τ_2 was presented from a second order exponential decay function ($c(t) = c_0 + A_1 e^{-t/\tau_1} + A_2 e^{-t/\tau_2}$) over the data within 1-100 ps.

[‡] τ was obtained from the fitting of a first order exponential decay function ($c(t) = c_0 + A e^{-t/\tau}$).

Figures
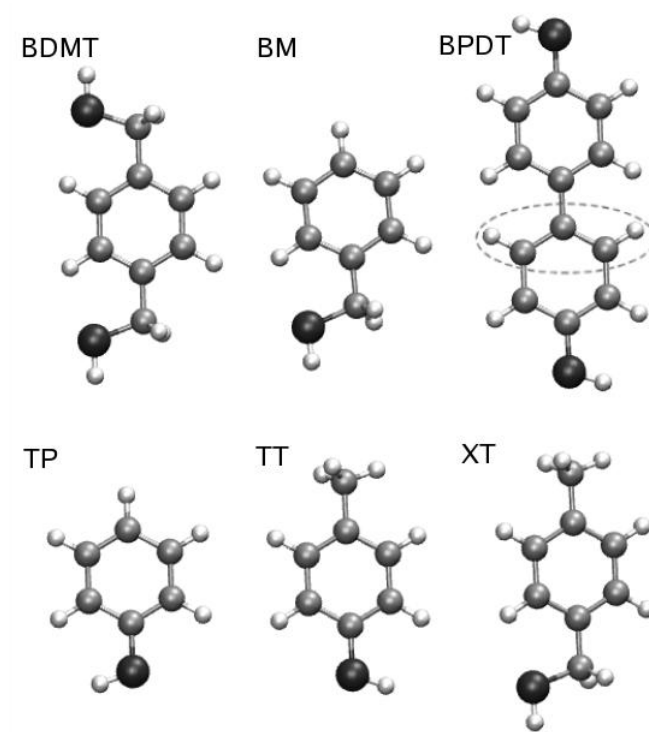
Figure 3. Structures and abbreviations of arylthiol molecules modeled in this work. 1,4-benzenedimethanethiol (BDMT), benzylmercaptan (BM), biphenyldithiol (BPDT), thiophenol (TP), 4-methylbenzenethiol (TT) and 4-methylbenzylthiol (XT).
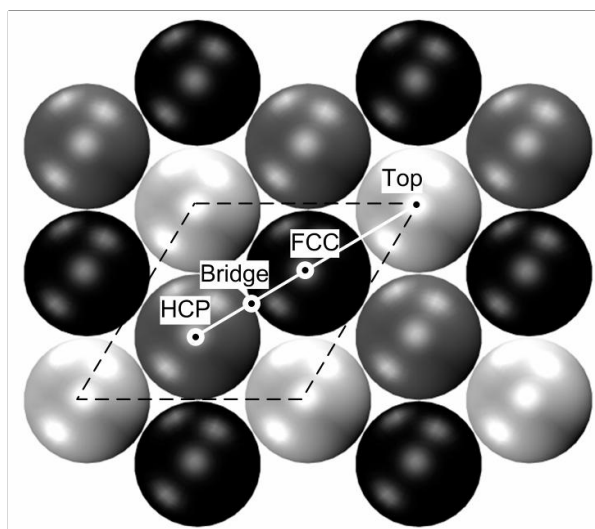
Figure 4. Schematic presentation of the lattice sites on Au(111) surface. Light gray, dark gray and black beads represent the Au atoms on the first, the second and the third layers, respectively.
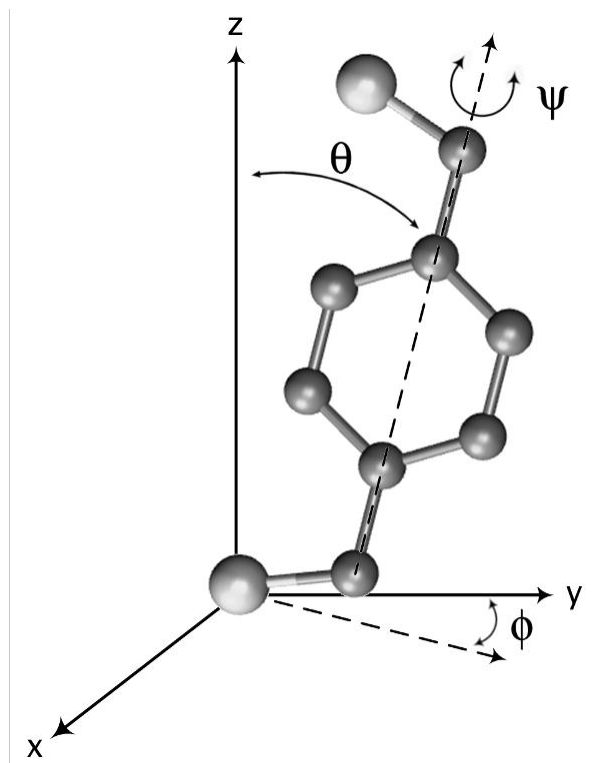
Figure 5. Three basic angles describing the conformation of self-assembling molecules with respect to the substrate.
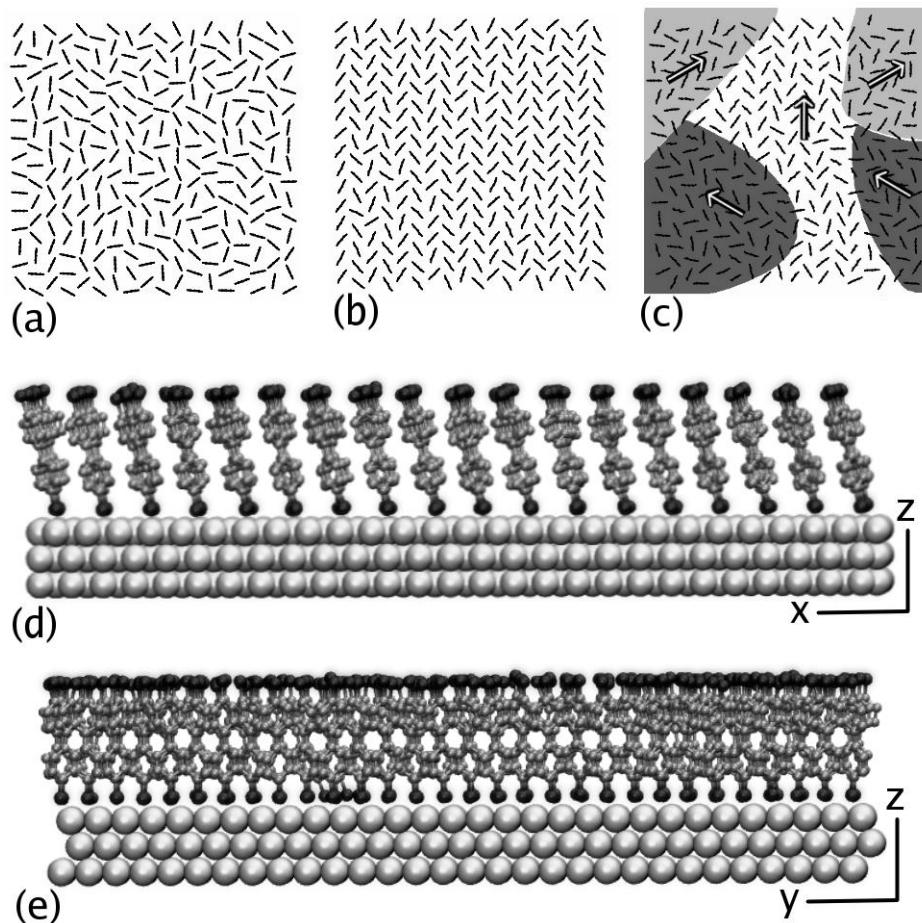
Figure 6. (a) Views of *xy*-plane at (a) initial and (b) equilibrated configurations for SAM of BPDT and (c) TP on Au(111) surface. Three areas are highlighted based on the orientation of the herringbone structure: 0°, 60° and -60° orientations are displayed on white, light gray and dark gray backgrounds, respectively. The BPDT atoms that are used in producing the image are those enclosed by the dashed ellipse in Figure 3. Views of (d) *xz*- and (e) *yz*-planes for the equilibrated SAM of BPDT on Au(111).
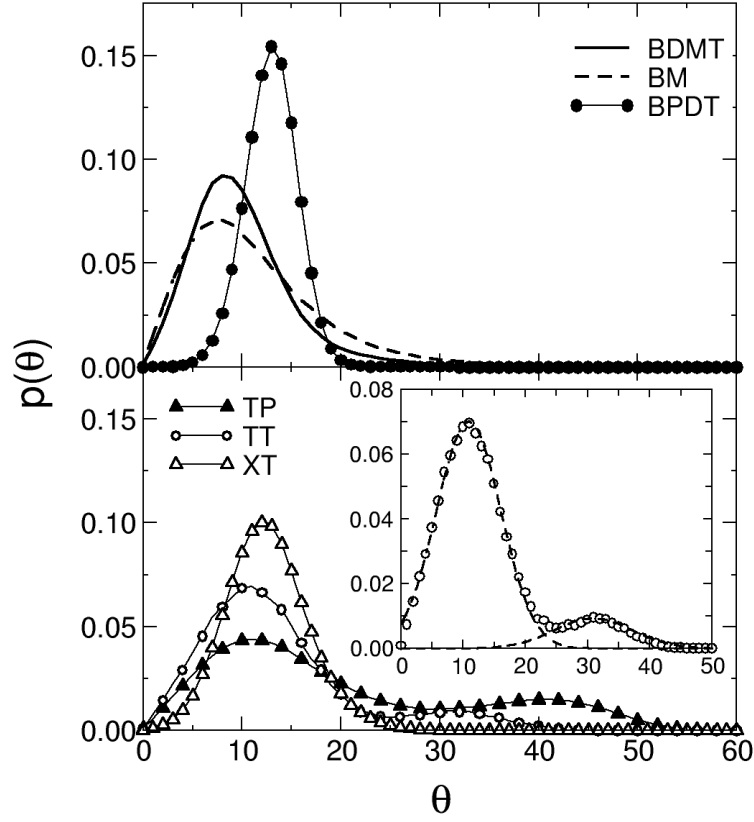
Figure 7. Probability distribution functions for the tilt angle (θ). (a) BDMT (line), BM (dashed line) and BPDT (filled circles). (b) TP (filled triangles), TT (open circles) and XT (open triangles). Dashed line in the inset shows Gaussian function fits to the TT.
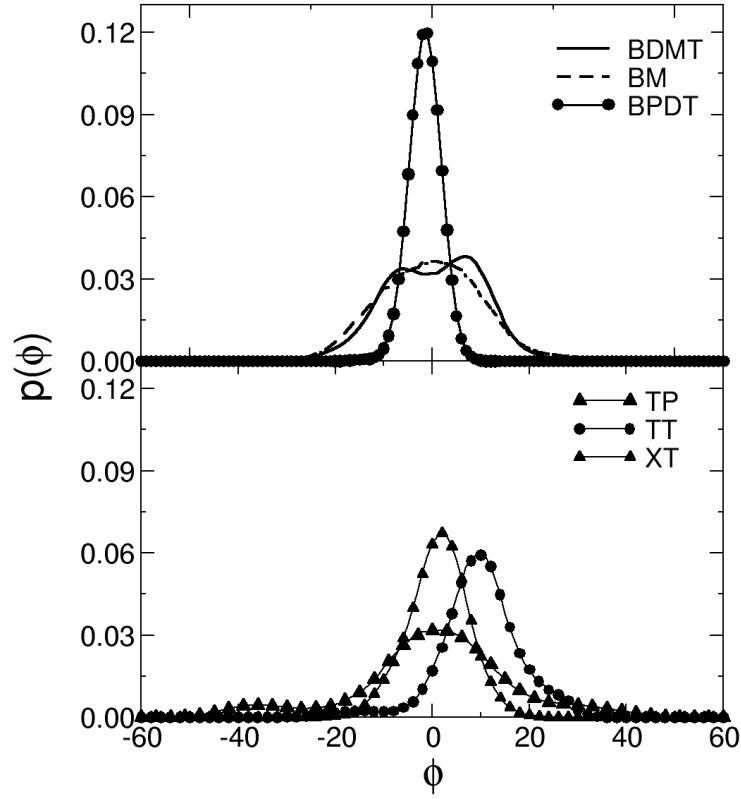
Figure 8. Probability distribution functions for the azimuthal angle (ϕ). (a) BDMT (line), BM (dashed line) and BPDT (filled circles). (b) TP (filled triangles), TT (open circles) and XT (open triangles).
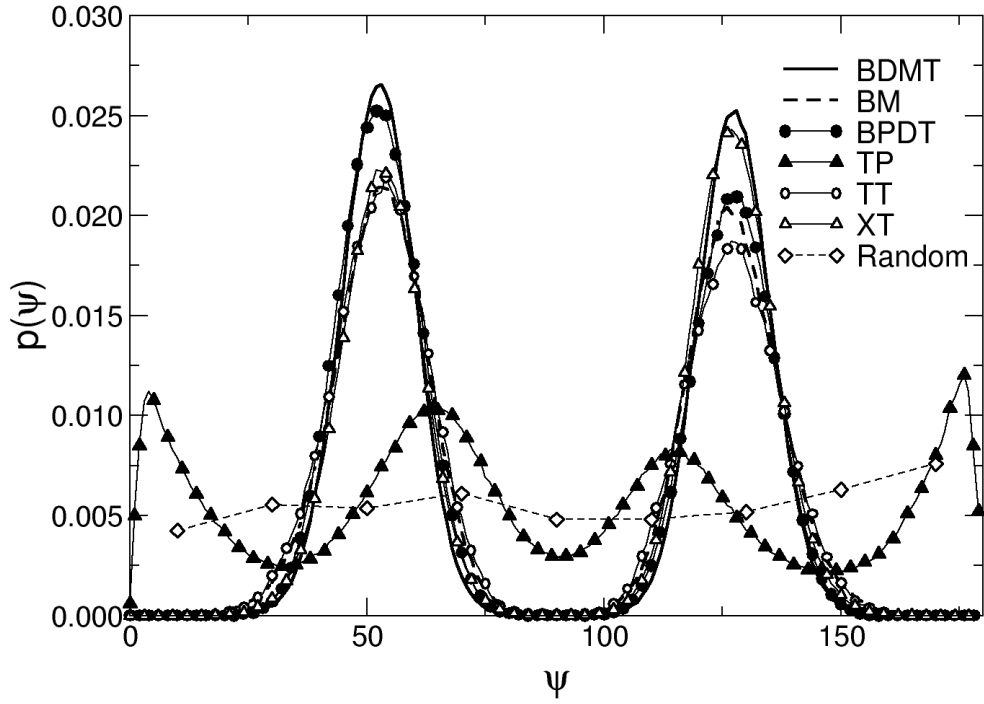
Figure 9. Probability distribution functions of the twist angle (ψ). BDMT (line), BM (dashed line), BPDT (filled circles), TP (filled triangles), TT (open circles) and XT (open triangles). The dashed line with diamond symbols represents the initial random distribution of ψ.
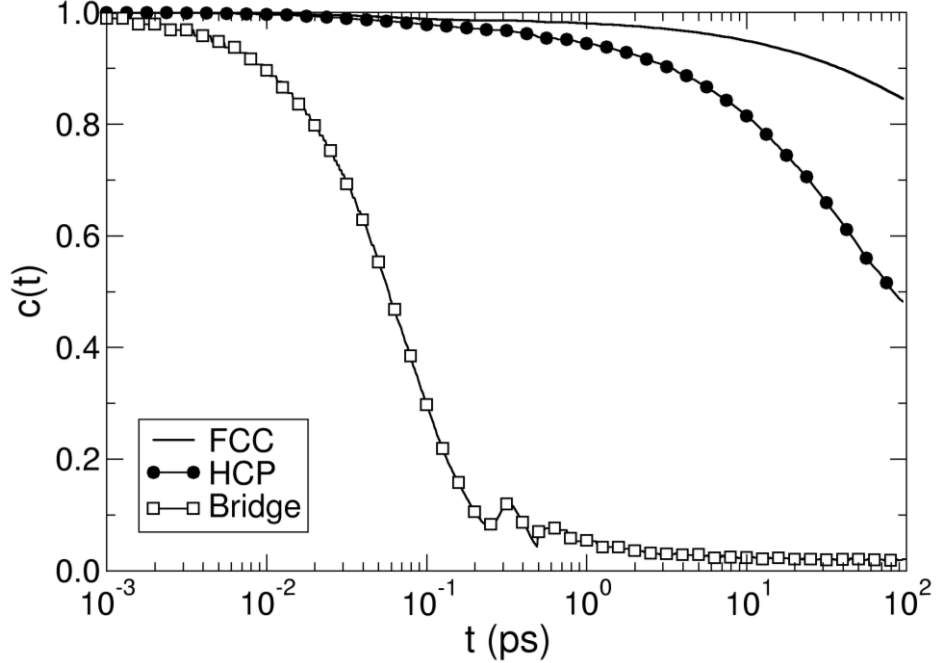
Figure 10. Time correlation functions ($c(t)$) of sulfur atom positions for the SAM of BM at the three observable sites on Au(111). FCC (line), HCP (filled circle) and *Bridge* (open square).

27
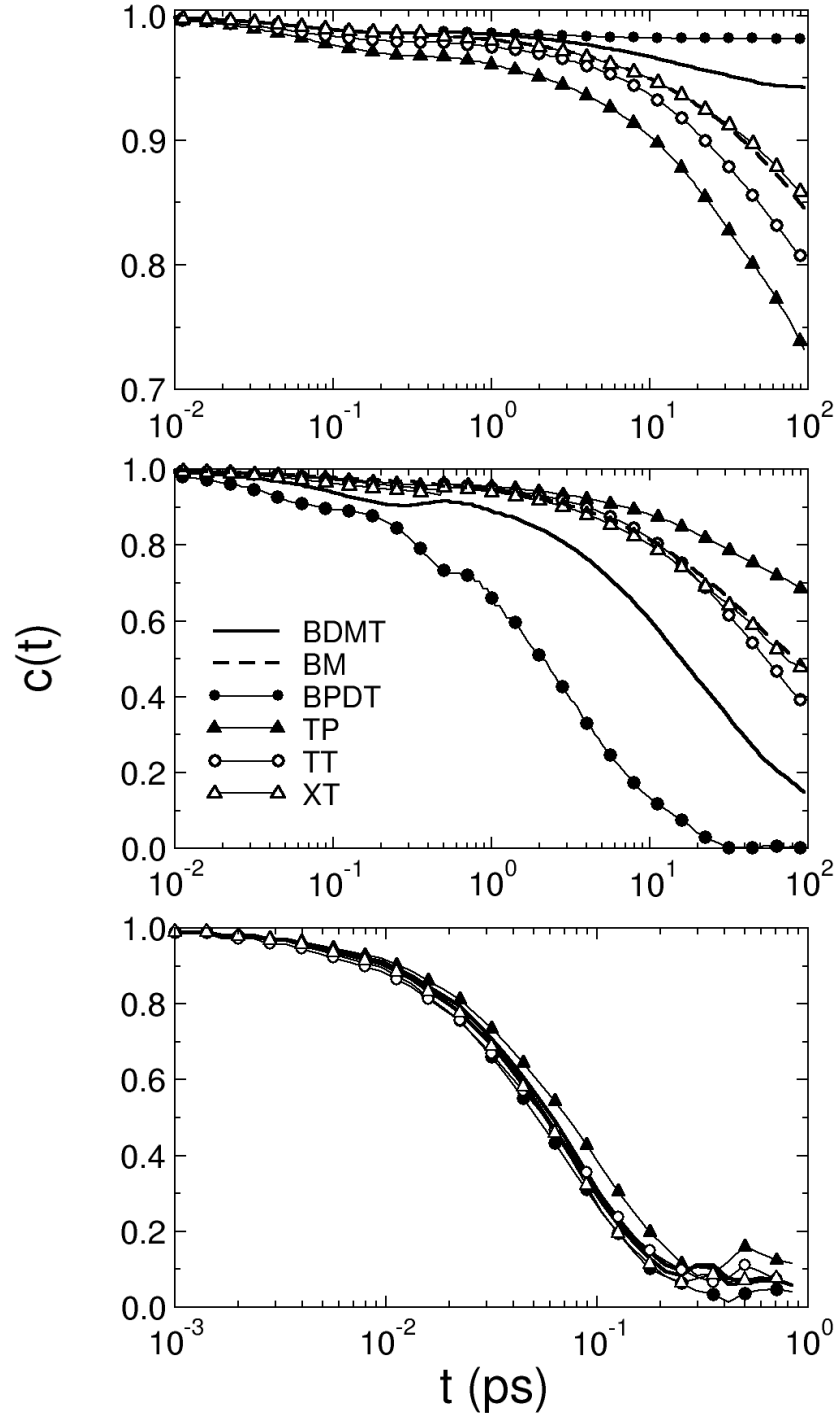
Figure 11. Time correlation functions ($c(t)$) of sulfur atom positions for SAMs at (a) FCC, (b) HCP and (c) *Bridge* sites of Au(111) surface. BDMT (line), BM (dashed line), BPDT (filled circles), TP (filled triangles), TT (open circles) and XT (open triangles).
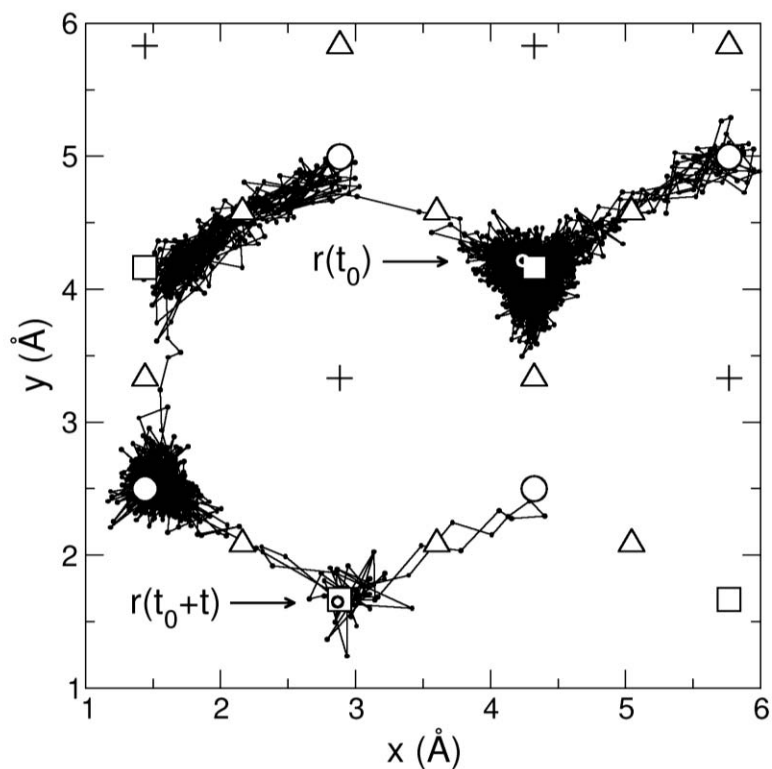
Figure 12. Trajectory of a TP head group over 500 ps of simulation. FCC, HCP, *Bridge* and *Top* sites were represented by circles, squares, triangles and pluses, respectively. The initial and final coordinates are indicated.
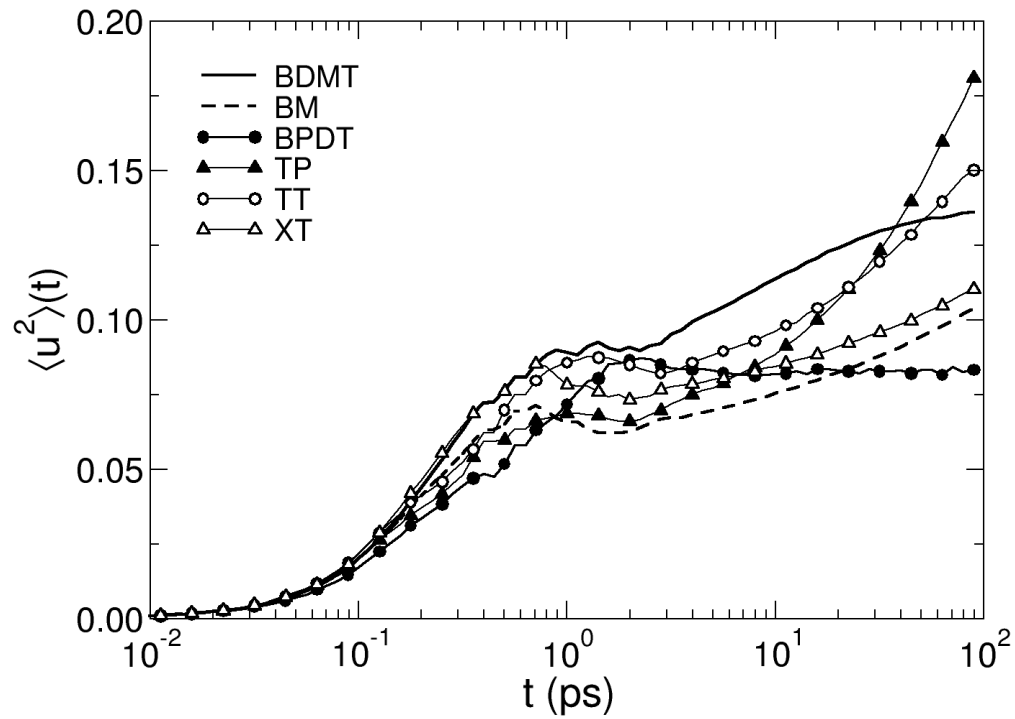
Figure 13. Weight averaged mean square displacement ($\langle u^2 \rangle(t)$) of self-assembling molecules versus time. BDMT (line), BM (dashed line), BPDT (filled circles), TP (filled triangles), TT (open circles) and XT (open triangles).
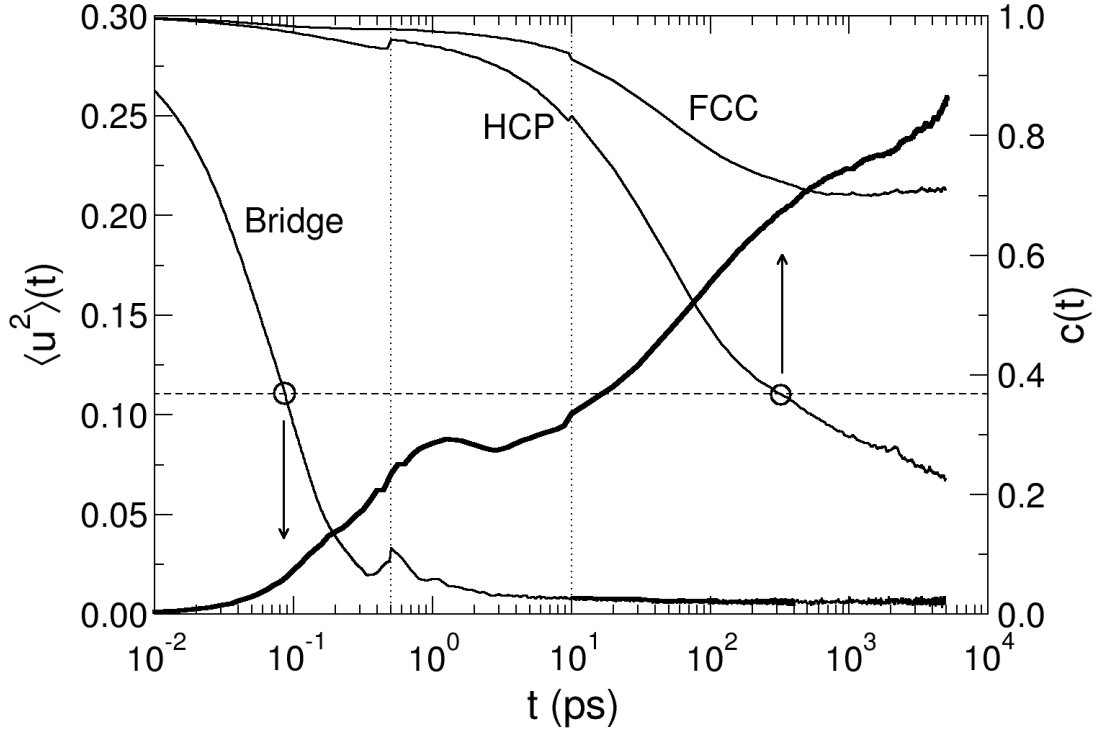
Figure 14. Overlaid plots of $\langle u^2 \rangle(t)$ (thick line) and $c_i(t)$ (thin lines) for TT. The curves were obtained by combining the plots computed using trajectories collected at different intervals (i.e. $t < 0.5$ ps from 0.001 ps, $0.5 < t < 10$ from 0.1 ps and $t > 10$ from 10 ps intervals). The vertical dotted lines represent the points where the data were joined together. Horizontal dashed line is $y = 0.368$ (i.e., e^{-1}). Intersection points of $c_i(t)$ with the horizontal line were encircled and changes occurring in $\langle u^2 \rangle(t)$ at that time range were pointed with arrows in order to guide the eye.

2.2.2 Probing Adhesive Interactions of Self-Assembled Monolayers by Simulating Force-Distance Measurements in Atomic Force Microscopy.

Introduction

Forces-versus-distance measurements using Atomic Force Microscopy (AFM) has become instrumental in surface science, colloidal chemistry, materials engineering and molecular biology.[48] They provide accurate information on surface and intermolecular forces that are difficult to obtain by other means. Self-assembled monolayers (SAMs) have become model systems for the force-distance measurements since they easily form highly ordered and densely packed monolayers, thus enabling the measurement of forces between chemical groups.

31

AFM tip as well as the substrate can be coated by the self-assembly of thiols on gold. This approach allows measuring the forces between various chemical groups including methyl, carboxyl, hydroxyl, amide and amino.[49-53]

The experimental measurements of force-distance curves in SAMs of thiols on gold surfaces have yielded conflicting results. Besides the experimental errors, the inability to fully characterize the tip and the surface of the SAMs right prior to and during the experiment could be a major contributor to the inconsistent measurements.

In this effort, we aimed to investigate the effect of SAM configuration on the adhesive surface forces by calculating the force-distance curves obtained with a gold tip on SAMs of dithiols at two different experimentally observed stable configurations: standing-up or striped phases. Standing-up phase is formed when the molecules stand with their head groups in contact with the substrate while the tail groups are positioned away from the substrate along the normal to the surface. In the case of a striped phase both the head and tail groups are in contact with the substrate. We further investigated a possible disordered phase and a SAM in standing-up configuration but when the tip carried some residual dithiols. The former might form if the SAM was formed improperly as well as if a properly formed SAM is exposed to some external field such as electrical current. The latter case is perhaps more representative of a standard force-distance measurement since the tip is exposed to the SAM surface prior to performing the intended force-distance measurement. We investigated the nature of the force curves and how the forces are developed at each scenario.

Model and Simulation Protocol

We briefly explain the model and refer the reader for further details to our earlier work. We used General Amber Force Field (GAFF)[29] to describe the intramolecular and intermolecular interactions of arylthiol molecules. Au-Au interactions were neglected by excluding them from the neighbor list and Au atoms were held steady by setting the force imposed by organic molecules to zero. The intermolecular interactions between self-assembling molecules and Au atoms were described by the Dreiding Force Field (FF)[31] with optimized parameters.[32] To describe these non-bonded van der Walls interactions, we used an exponential-6 form.

$$E_{ij} = D\left[\left(\frac{6}{\zeta - 6}\right)\exp\left(\zeta\left(1 - \frac{R_{ij}}{R}\right)\right) - \left(\frac{\zeta}{\zeta - 6}\right)\left(\frac{R_{ij}}{R}\right)^{-6}\right] \qquad (1)$$

Here, D is the depth of the energy well, R_{ij} is the distance between atoms, R is the distance at energy minimum and ζ is a dimensionless constant, were the default value of $\zeta = 12$ was used. We used Dreiding force field (FF) parameters that were optimized by Jang et al.[32] for the interactions between Au atoms and those in the molecules.

Au(111) slab was created in an FCC lattice arrangement with a lattice spacing of 4.0782 Å after the 111 plane was oriented along the z-axis. The resulting Au(111) slab consisted of a total of 4860 atoms arranged in 27 ×30 × 6 in x, y and z-directions. The tip was formed in the same lattice structure with a 10 nm diameter (see right panel in Figure 15).

The arylthiol molecules were built using the LEAP module in AMBER[37]. Point charges on atoms were calculated using the AM1-BCC method[38] which was parameterized to reproduce HF/6-31G* RESP charges.

In standing-up phase, the experimentally suggested arrangement on an ideal surface of Au(111) is the assembly of organothiols at ($\sqrt{3}\times\sqrt{3}$)-R30° triangular lattice with S atoms being positioned on the FCC (i.e. 3-fold hollow) site.[39] A monolayer was formed by accordingly placing 270 organothiol molecules for the modeling of the standing-up phase. However, the molecular arrangement for the striped phase is dependent on the shape, size and the chemistry of the self-assembling molecule unlike in the standing-up phase. Experimental data for the arrangement of molecules in SAM of BPDT in the striped phase is not available. *4-methyl-4'-mercaptobiphenyl* (MMB) is compound that differs from BPDT only with a thiol group instead of a methyl group. Therefore, it is expected that the molecular arrangement of SAMs of MMB molecules is a good approximation to that of BPDT. The structure of MMB SAMs for the striped phase was reported as conforming a ($8 \times 2\sqrt{3}$) unit cell with dimensions of 23.08 ×10 Å and containing four molecules per unit cell.[45] The head to head configuration of molecules results in S-S distances of about 2.1 Å (about the equilibrium distance of disulfide bond). Unlike MMB, BPDT has another thiol group at the tail position which enables the possibility of the formation of disulfide-like bonds between tail groups as well as head and tail groups. Therefore, we used Morse bond potential to describe the bonds between neighboring sulfur atoms.

$$E_{Morse} = D\left[1 - e^{-\alpha(r-r_o)}\right]^2 \quad (2)$$

D is the depth of the potential well, α is the stiffness parameter and r_o is the equilibrium bond distance. The parameters are D = 14.0 kcal/mol, $\alpha = 3.44$ Å^{-1} and $r_o = 2.1$ Å.[54] This approach a

stable structure that follows the molecular arrangement of MMB SAM as shown in Figure 15. The unit cell dimensions as well as tilting of molecular axis with respect to vertical axis by a small angle are preserved. Since both thiol groups are at contact with the gold surface, molecules bend along their molecular axis. In addition, the neighboring sulfur atoms are found at either at ~2.2 or ~4.0 Å separation. They are either at equilibrium separation of a S-S bond (2.1 Å) or at equilibrium separation of van der Walls interaction (4.0 Å). During the course of simulations the S-S separations alter between these two distances. Even though our approach has yielded a stable structure consistent with that of MMB, it could be one of other reasonable striped phases for BPDT. Thus, we consider this structure as an *approximate* striped phase that yields a plausible surface coverage for BPDT.

The dimensions of the simulation box for all cases except the striped phase were set to be 77.86, 74.92 and 200.00 Å in x, y and z directions, respectively. In the case of the striped phase, x and y dimension were set at 69.21 and 69.93 in order to accommodate the unit cell dimensions for the striped phase (i.e. 23.08 ×10 Å). Setting a very large box dimension in the z-direction rendered true 3-dimensional periodic boundary conditions as effectively 2-dimensional.

The MD simulations were performed using LAMMPS (Large-scale Atomic/Molecular Massively Parallel Simulator).[40] Lennard-Jones and Coulombic interactions for pairs of organic atoms were computed using a switching function with inner and outer cutoffs of 14 and 16 Å, respectively, whereas the cutoff for the interactions of Au-organic atom pairs was set to be 14 Å. The long range Coulombic interactions beyond the cutoff (reciprocal sum) were calculated using the particle-particle particle-mesh Ewald (PPPM) solver[41] with a precision value of 1.0×10^{-4}. The equations of motion were integrated using the Verlet algorithm[42] with a time step of 1 fs. The SHAKE algorithm was applied to all hydrogen atoms. Temperature in a canonical (NVT) ensemble was controlled using the Nosé/Hoover thermostat.[43, 44]

The equilibrated structures of SAMs in standing-up and striped phases that were equilibrated in the same manner as previously explained are shown in Figure 16 (a) and (b).[55] In order to create a disordered assembly, the SAM at the standing-up phase was artificially melted as follows. The monolayer first was sandwiched between gold surfaces with a ~15 Å gap by reducing the simulation box size in z to 27 Å. The temperature was raised to 900 K and the monolayer was melted over 400 ps of simulation in NVT ensemble. In addition, in order to expedite the melting the S-Au interaction type was replaced with C-Au at this stage.

Subsequently, the temperature was lowered to 300 K and the box size and the interactions were reset to the original values. The resulting structure (shown in Figure 16 (c)) will be discussed in the next section.

The tip was displaced up and down in a quasi-equilibrium fashion to simulate its approach and withdrawal. Subsequent to displacing the tip along the z-direction with a selected speed over an incremental distance of 0.1 Å, the simulation was run at the new position for the same number of simulation steps needed for the incremental displacement. At this stage, forces applied on the tip atoms were collected and then averaged to yield a single data point. The collection of such data points at varying displacements produces the force-distance curves. This approach has resulted in reproducible force measurements as exemplified in the next section.

Our model for SAMs of alkanethiols on Au(111) involves several assumptions and approximations besides the standard approximations in MD simulations. Here we briefly discuss their possible consequences. The representations of S-Au and molecule-molecule interactions are critical because the structure of SAMs is determined by the strong interactions between the head groups and the metal substrate besides the inter-chain interactions among self-assembling molecules. The SAM structure comes about due the interplay between the two interactions types, which are commonly described by the binding energy and the SAM formation energy. Our earlier work[55] based on the same approach has shown a good agreement in the binding energy to the results of Density functional Theory (DFT)[32] and helium beam reflectivity and temperature-programmed desorption experiments[33]. Another approximation is keeping the Au surface rigid. DFT studies of Kim et al.[19] has shown that keeping the Au atoms frozen had no discernible effect on the SAM dynamics, which should be sensitive to surface characteristics. An additional assumption was that the Au atoms carried no charge. When thiol molecules are deposited on the Au surface, it is expected that the Au atoms on the surface get polarized and be subject to some charge distribution. However, since the S-Au interaction is represented with a very strong non-bonded interaction, any contribution of the resulting electrostatic interaction to the overall potential should be negligible.

Results

One factor to consider in performing force-distance measurements is the penetration depth of tip into the sample. It is a difficult parameter to control in AFM experiments because after the sudden jump into direct contact with the surface, only force applied at is being

controlled. For instance whether the tip would penetrate through a lipid bilayer has a probability that depends on the force applied and the velocity of the tip.[56] In our model since we control the displacement the tip, we can study the effect of the penetration depth. Therefore, we start our analysis of force-distance curves by varying the level of approach into the SAM in standing-up phase.

When the tip was brought to 2.4 Å from the surface in (a), the approach and withdrawal curves overlap, because the tip was not wetted at this separation. The well in the force curve is due to the strong favorable interactions between the sulfur atoms on the surface and the gold atoms in the bottom layer of the tip. The wetting occurred with 16 thiols being lifted with the tip when the tip was brought to the same z position as the surface of the SAM. The force curve shows another but a deeper well corresponding to the second layer of atoms in the tip. The approach and withdrawal curves are no longer overlapping due to the thiol groups that are attached to the tip. This can be interpreted as an inelastic deformation of the SAM. As the tip was penetrated by 2.4, 4.7 and 7.1 Å, the layers that are higher in the tip become available to the sulfur atoms on the surface. However, the effects of the layers are clearly visible only until the third one, because the repulsive interactions between the atoms in the lower layers of the tip and those of SAM dominate over the attractive interactions as the tip penetrates deeper into the SAM. At each positive penetration the tip collected 16, 36, 56 and 98 dithiol molecules for the penetration depths of 0.0, 2.4, 4.7 and 7.1 Å, respectively. One important observation is that the maximum force (F_m) of withdrawal does not change with the penetration depth (or the number of dithiols lifted with the tip) after 0 penetration. At this penetration level the second layer at the bottom of the tip is approximately at the equilibrium interaction distance with the SAM surface.

We studied the effect of the tip speed (from 0.5 to 0.02 Å/ps) at the approach and withdrawal stages on a SAM in standing-up phase (Figure 20). During approach all curves overlap for the first two valleys (A and B). Later the effect of speed presents itself. The hill between B and C diminishes as the speed is lowered indicating that SAM molecules can be moved away easily. By end of equilibrium stage all curves merge. Withdrawal curve does not have velocity dependence in the range of speeds we applied. However, it is worthy of mentioning that in actual force-distance measurements the tip is moved at a much slower rate than what we can practically achieve by MD simulations.

Figure 21 presents the approach and withdrawal curves for the lower coverage striped phase. We do not observe four valleys and peaks as in the case of standing-up phase. The depth of the first well is much shallower than that of SAM in standing-up configuration due to small density of molecules on the surface. Striped phase has a surface density of only 57.6 Å^2/molecule compared to 21.6 57.6 Å^2/molecule in standing-up phase. Following another shallow well at 3 Å the force climbs rapidly since the molecules get squeezed quickly within a small space between the tip and the gold surface. At the withdrawal stage force goes through a minimum and then levels off while either head or tail groups attach to the tip get lifted of the gold surface. The leveling occurs because as one end of a molecule id lifted for more than a couple of angstroms, the attractive interactions quickly drop. Later at separation of around 10 Å, a deeper well (11 nN) is observed before force eventually vanishes at d>15 Å. This secondary well is a reflection of other molecules that are bonded to those primarily attached to the tip being striped off from the surface as seen in Figure 17(b).

We now investigate the force-distance curve for perhaps a hypothetical case of a disordered assembly of BPDT molecules. Even tough there has been no report, to the authors' knowledge, that a stable disordered assembly has been formed, it may be possible to obtain such an assembly. The S-Au bonds, which have already been demonstrates as being unstable in various experiments, could be broken collectively by an external stimulus.[20-23] For instance, Paramanov et al. have shown that the thiol-gold interface in an SAM of alkanethiolates can be disrupted by applying a negative bias to the tip that was held slightly above the SAM.[57] They proposed that thiols groups attached to and lifted with the tip after the S-Au bonds were broken via an oxidative cleavage induced by the negative bias. After disrupting the S-Au interface molecules may rearrange their conformations and get trapped in a meta-stable disordered structure.

Before discussing the features of force-distance curve for a disordered assembly, we examine the structure of the assembly formed as explained earlier. One realizes upon close observation of its structure that this assembly is similar to the striped phase at gold surface because dithiols cover a large amount of the surface by taking a lying down conformation. 60 % percent of the molecules with a direct contact to the surface were found to be lying-down and the remaining had only one of their thiol groups on the surface. The surface densities of lying-down and standing-up molecules are 97.2 and 145.8 Å^2/molecule, respectively. The combined surface

density in the disordered assembly is 58.3 Å^2/molecule, which is about the surface density of the SAM in the striped phase (i.e. 57.6 Å^2/molecule).

In the approach stage force narrowly goes to attractive region, because the molecules that interact with the tip have mostly no direct contact with the surface. These molecules do not form bridges between the tip and the surface that give rise to the attractive forces as in ordered SAMs. However, force clearly goes deep into the attractive region at the withdrawal stage. The features that were seen for the SAM in the standing-up configuration are observed noticeably at A' and B'. To understand the changes in the molecular conformations at the approach, equilibrium and withdrawal stages we calculated the order parameter.

$$S = \left\langle \left| \cos(\theta) \right| \right\rangle \qquad (2)$$

where θ is the angle between molecular axis and normal to the substrate (z-axis). Since the BPDT molecule is symmetric we do not distinguish the head and tail group positions. We analyze the order parameter for molecules above those that are lying down at the surface in Figure 23 (a). The assembly appears initially to be nearly entirely disordered with a small bias towards the vertical alignment (i.e. $S = 0.57$ which is close to $S = 0.5$ for the complete disorder). As the tip was moved toward the assembly S increased first and then decreased signifying that the tip oriented the molecules vertically when at slightly above the assembly and disoriented them when inserted into the assembly. Meanwhile, S for the lying-down molecules increases from approximately zero indicating some orientation when the tip gets to a close proximity (Figure 23 (b)). This increase shows that one of the thiol groups in some of these molecules gets attached to the tip. During the equilibrium S remains constant for both types of molecules. However, as soon as the tip is lifted by a few Angstroms S returns to its original value for the lying-down molecules. Contrarily, S increases up to 0.75 within 7 Å and remains above the original value as the tip is retracted for the molecules above those that are lying-down. This result shows that there is a tip induced ordering in the disordered assembly.

In an experimental force-distance measurement, the tip is often brought to contact with SAM prior to intended approach and withdrawal stages. This leads to the gold tip to accumulate some residual thiols being present during the actual measurement. In Figure 24, we present the results of standing-up SAM when the tip with dithiols carried after a prior approach and withdrawal experiment was used. This tip had 73 BPDT molecules attached to it. During the

approach force never goes to the attractive region, rather it increases gradually until about 3 Å and then ramps up quickly in a similar fashion to the no residual case but about 5 Å earlier. Apparently, the residual molecules are forced into the monolayer pushing the ordered molecules aside that screens the attractive tip-SAM interactions. Some of the residual molecules are forced to the higher layers in the tip (see Figure 17 (d)). During the equilibration some of the molecules in SAM get flattened while others manage to establish attractive interaction with the tip. For this reason, force shows two attractive valleys in the withdrawal stage at B' and A'. An interesting outcome of this measurement is that the maximum attractive force is three times higher when there are no residual molecules than the case with residual molecules on the tip. We will discuss the significance and possible consequences of this observation in the next section.

One key goal of this study was to understand how the structure of SAM affects the maximum adhesive force (F_m) as usually measured by AFM. F_m and the distance where it occurs (d_m) are tabulated in Table 2 for four cases studied.

TABLES

Table 7. Distance and depth of wells in force curves for the SAM of BPDT in standing-up configuration.

	Approach			Withdrawal	
	F (nN)	d (Å)		F (nN)	d (Å)
A	27	3.2	A'	23	3.3
B	46	1.0	B'	53	0.9
C	7	-1.5	C'	42	-1.5
D	-21	-3.3	D'	14	-4.0

Table 8. Maximum adhesive forces (F_m) and distance (d_m) for different assemblies studied.

	Approach		Withdrawal	
	F_m (nN)	d_m (Å)	F_m (nN)	d_m (Å)
Standing-up	46	1.0	53	0.9
Striped	5	3.1	11	11.0
Residual	0	-	17	3.3
Disordered	4	2.9	27	0.6
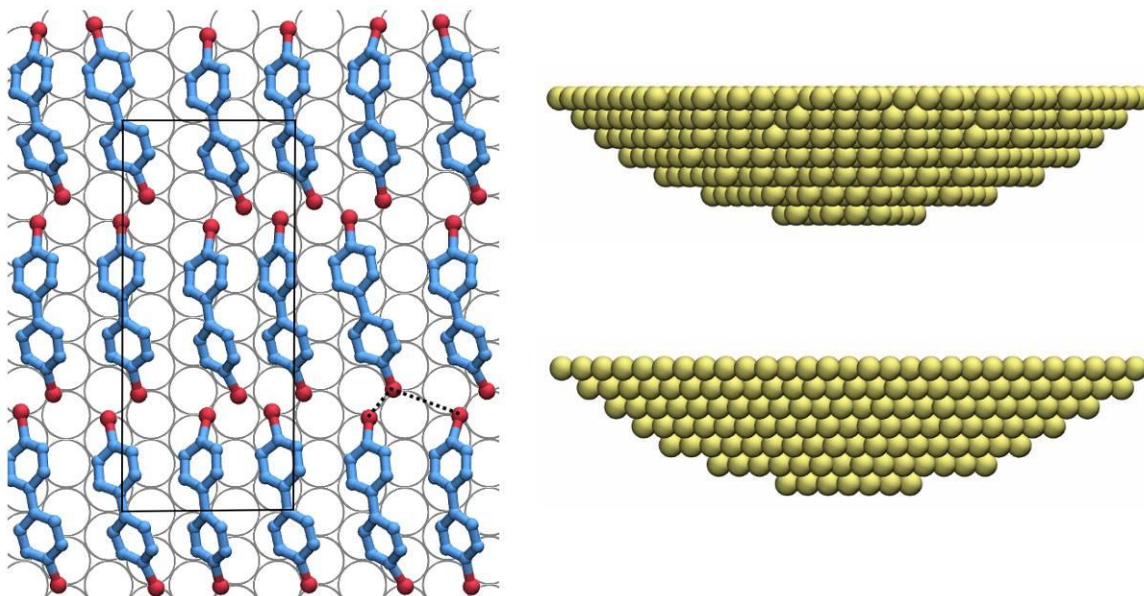
Figure 15. (Left panel) Views through *x-y* plane of the striped phase. Carbon and sulfur atoms are shown in blue and red, respectively. Hydrogen atoms were omitted for clarity. The rectangle represents the initial unit cell with dimensions of 23.08 ×10 Å. The dashed lines exemplify two different separations (~2.2 and ~4.0 Å) of neighboring sulfur atoms. (Right panel) Views of the tip through *x-z* and y-*z* planes at the top and the bottom, respectively.
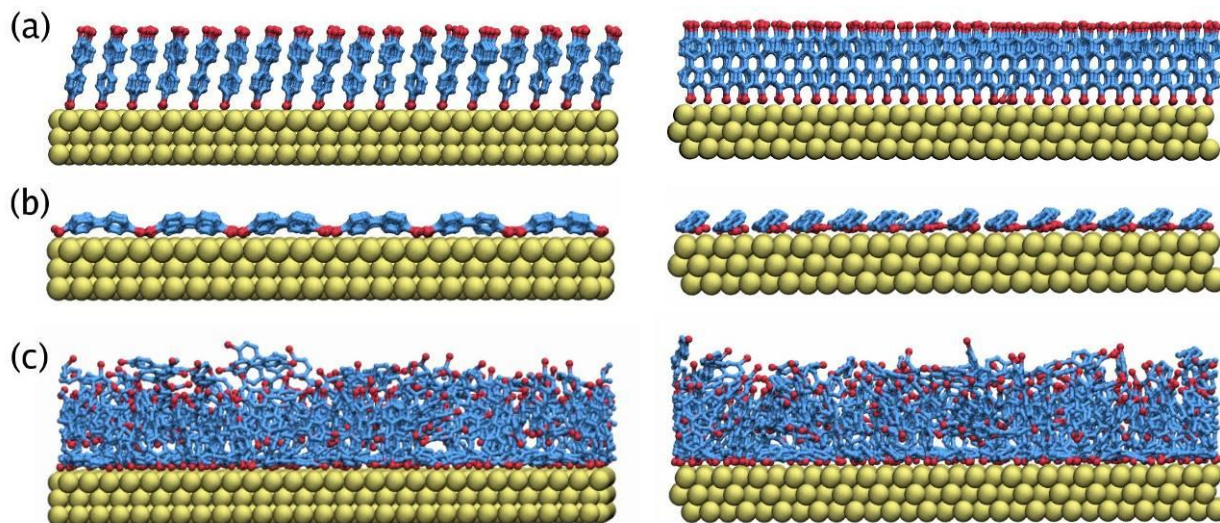
Figure 16. Views through *x-z* (left) and *y-z* (right) planes for (a) standing-up, (b) striped and (c) disordered BPDT assemblies. Carbon, sulfur and gold atoms are shown in blue, red and gold, respectively. Hydrogen atoms were omitted for clarity.
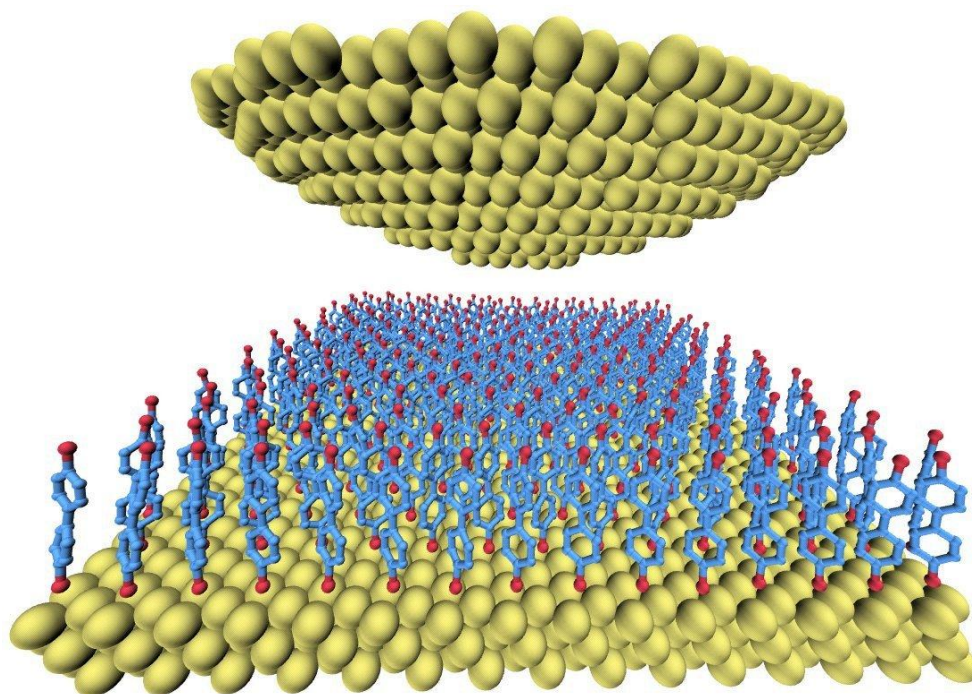
Figure 17. A view of the SAM in standing-up phase with gold tip.
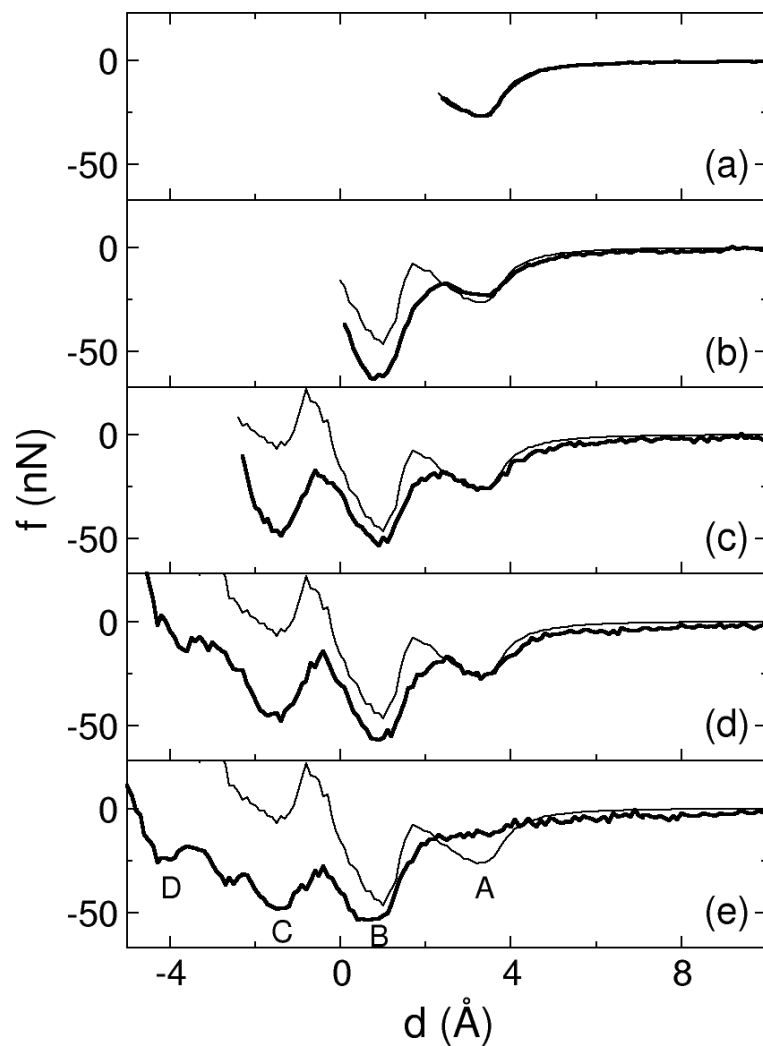
Figure 18. Force-distance curves at varying penetration depths: (a) -2.4, (b) 0.0, (c) 2.4, (d) 4.7 and (e) 7.1 Å. A negative penetration depth indicates no penetration. Thin and thick lines represent approach and withdrawal stages, respectively.
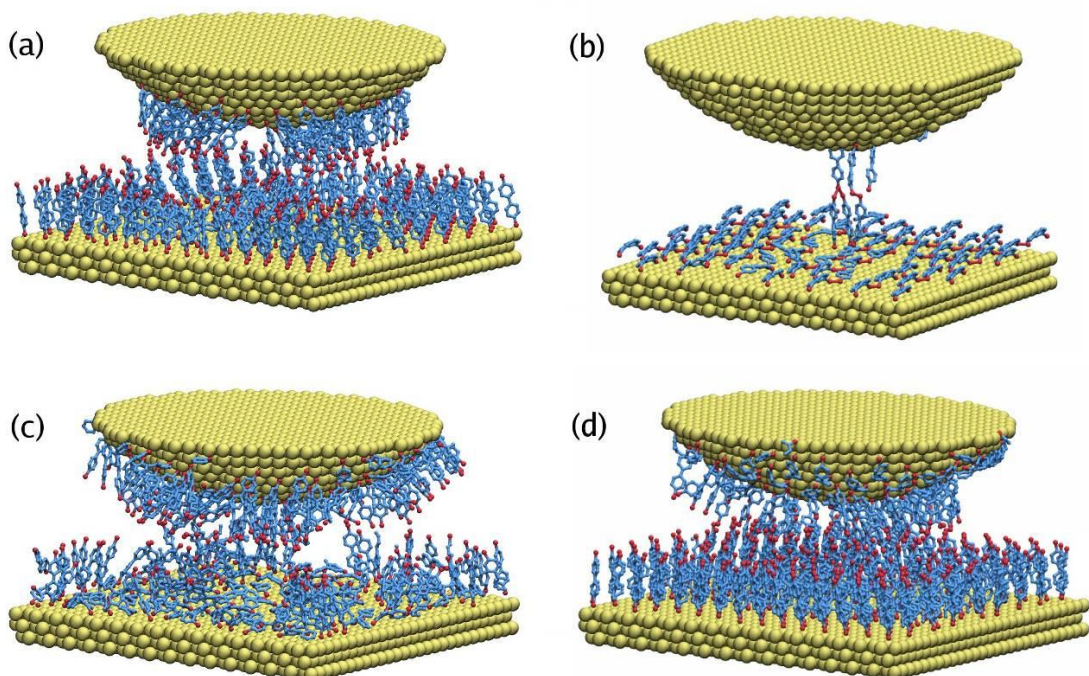
Figure 19.   Views of the system after the withdrawal of the tip for (a) standing-up, (b) striped, (c) disordered and (d) standing-up (with residual BPDT molecules on the tip) assemblies.
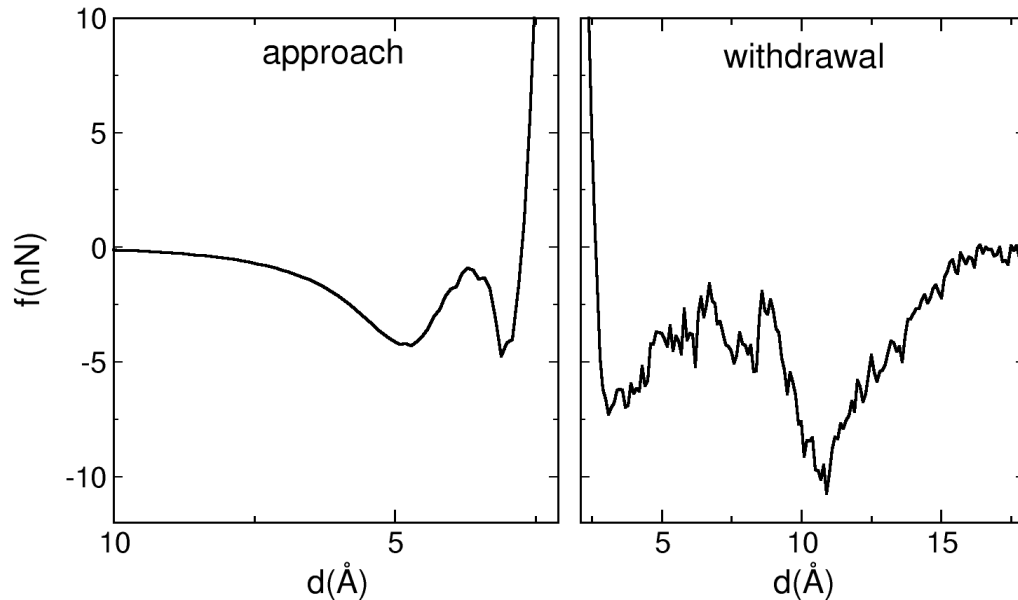
Figure 20.   Force-distance curves for the SAM at the standing-up phase at four tip movement speeds: 0.5 (thin line), 0.15 (dashed line), 0.05 (solid line) and 0.02 (solid line with circles) Å/ps. Approach, stationary and withdrawal stages are shown.
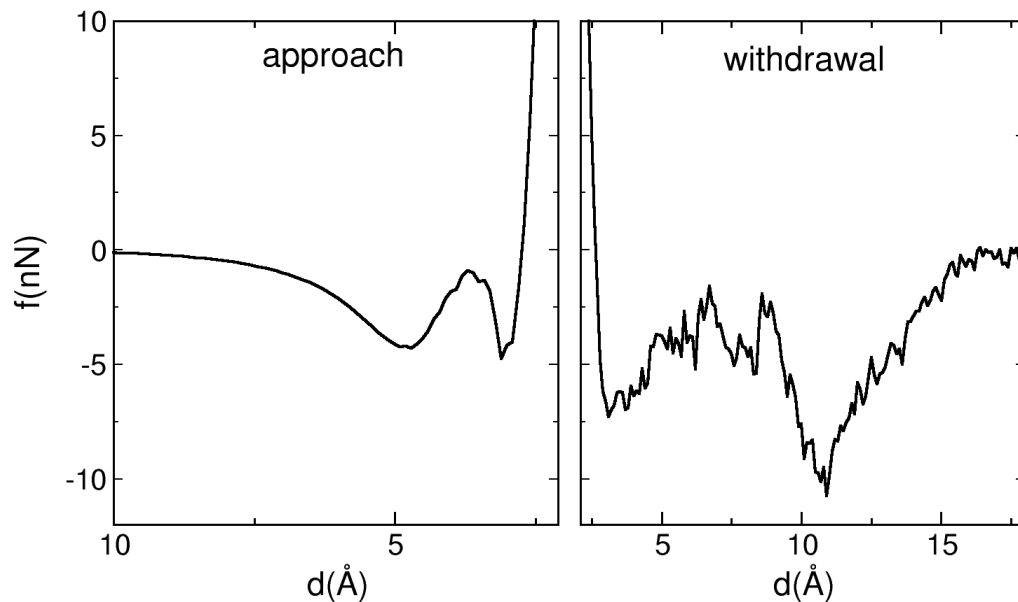
Figure 21. Force-distance curves for the SAM at the striped phase. Approach, stationary and withdrawal stages are shown.
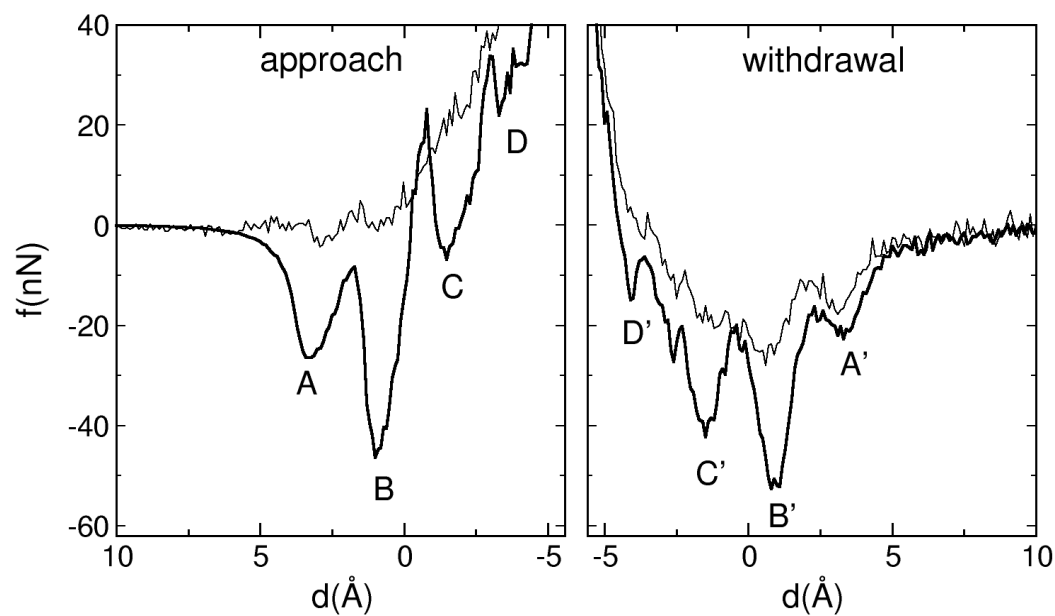
Figure 22. Comparison of force-distance curves of the disordered assembly (thin lines) to the SAM at the standing-up phase (thick lines). Approach and withdrawal stages are shown.
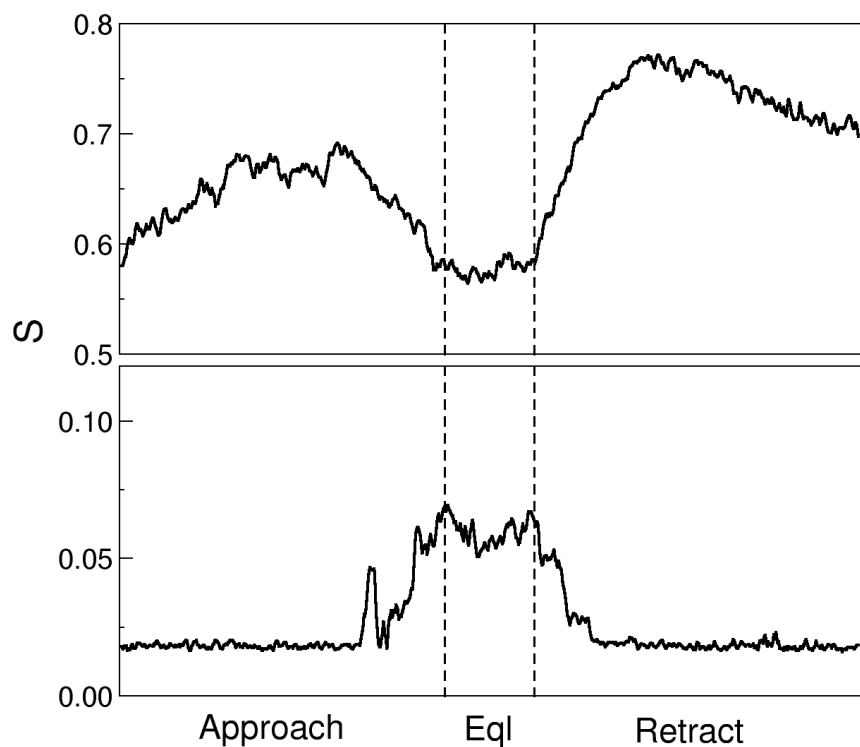
Figure 23. Order parameter for the disordered assembly calculated considering the lying-down molecules (lower panel) and the rest (upper panel).
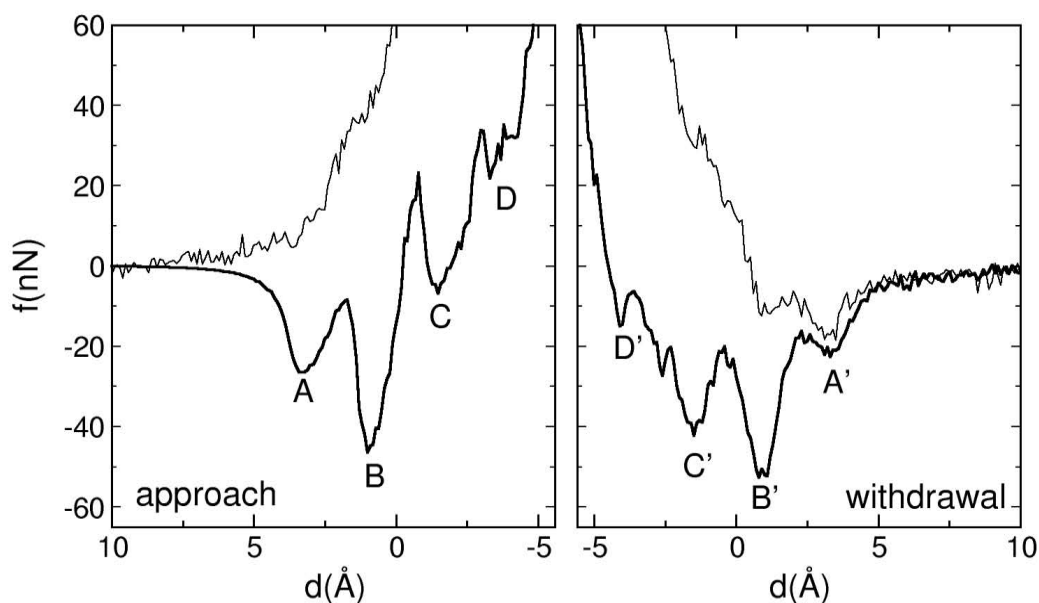
Figure 24. Comparison of force-distance curves of the SAM at the standing-up phase obtained with (thin lines) and without (thick lines) residual BPDT molecules on the tip. Approach and withdrawal stages are shown.

2.3 Self-Healing Materials

2.3.1 Coarse-Grained Molecular Dynamics Simulations of Self-Healing Polymeric Networks

Introduction

One of the challenges that material science is facing is to design smart materials that can sense the presence of a defect and actively repair the defected area. Such *self-healing* materials would significantly extend the lifetime and the usefulness of manufactured items [58] such as polymer matrix composites as replacements of metals, and cross-linked systems as adhesives or coatings.

The approaches addressing the self-healing phenomenon in materials science can be categorized in three classes: *healing with an embedded liquid*, *thermally activated solid phase healing* and *healing of projectile puncture* [59]. The first approach involves embedding capsules containing a reactive healing liquid (e.g., resin) that rupture and release the liquid upon deformation. While it has proven to be successful in repairing the damaged area it has stability issues while processing and the available liquid payload capacity is often limited for various reasons. The second approach provides an improved performance after every cycle of heating, but there is a requirement of external heat supply that makes the process non-autonomic. The third approach has gained recent interest perhaps because it neither requires an external intervention nor has stability issues. It has been shown that the target film (based on ionomers such as copolymers of ethylene and methacrylic acid) that was penetrated by a projectile with a high speed is healed to an airtight condition almost instantly. Essentially, the penetration of the projectile causes localized heating near the puncture which then closes upon itself to heal. The mechanism behind such a self-healing process after ballistic penetration involves two transformations. First, the film which has been locally melted due to heat dissipation re-crystallizes and solidifies. Later, the reordering of the physical cross-links takes place. These physical cross-links, according to Eisenberg–Hird–Moore model [60], are primary aggregates that consist of several ion pairs known as *multiplets*. These multiplets bring several chains together bound by ionic interaction creating physical cross-links. Calorimetric studies [61] have shown that the re-crystallization occurs rapidly while the reformation of the physical cross-links is a rather slow process. As a result, the material fully recovers after the latter process is complete.

Highly cross-linked epoxies or polyurethanes are a class of materials that can particularly benefit from a self-healing mechanism. While they possess a variety of appealing properties, two major shortcomings of highly crosslinked materials are their brittleness and low elongation, which are due to the limited degree of freedom available to the strands between the cross-linking points. The strands extend to their limits even with a small deformation and cause breaking of covalent bonds. Since the covalent bonds are non-reformable, any damage that is caused by impact or elongation will be permanent and cause formation of micro-cracks. For instance, cyclic mechanical loads result in accumulation of the micro-cracks which then leads to catastrophic failure.

The important question is: would a similar idea to that behind the healing of projectile puncture in thermoplastic ionomers apply to thermosets? It is known that the breaking of covalent bonds is responsible for reducing the impact resistance properties. The inherent toughness of the network is accommodated mainly by non-covalent interactions such as van der Waals and hydrogen bond interactions. Their effectiveness is due to their capability of breaking and displacing under stress to absorb impact energy. However, under high energy impact conditions such weak interactions may not provide a sufficient level of strength in the material. Therefore, in theory, incorporation of stronger, yet reversible ionic bonds (i.e. two oppositely charged neighboring beads) into the polymeric matrix could be an alternative and effective approach to improve the impact properties. However, one needs to realize that a similar mechanism explained above for thermoplastic ionomers is an unlikely means for the highly cross-linked materials. First, there will not be re-crystallization since the low degree of freedom in the material prevents crystallization. Secondly, the formation of multiplets is hindered also due to the cross-linked nature of the polymer.

For cross-linked systems with embedded ionomers one could envision an alternative mechanism in which the multiplets are replaced by ionic pairs and the extent of repairing action is reduced primarily to the length scale of strands between cross-links. A temporary loss of the ionic interaction caused by deformation can be restored by the same or another pair of ionic groups. Moreover, the addition of ionic pairs which are stronger than van der Waals and hydrogen bond interactions, yet still reversible, could serve to increase the bulk material strength and the toughness. The soundness of this probable mechanism can suitably be studied using molecular modeling. Past molecular simulation studies of ionic polymers focused mainly on their

48

charge transport properties associated with applications such as polyelectrolyte membranes in fuel cells [62-64]. Accordingly, these modeling studies have primarily concerned with *solubility, conductivity* and *diffusivity* rather than *mechanical properties*.

Computational modeling of networked polymers has gained limited attention in contrast to their widespread use in many applications. Atomistic models of such systems include epoxy resins that were modeled using a single step cross-linking procedure [65] and poly(dimethylsiloxane) (PDMS) network where a dynamical cross-linking procedure was used [66]. Besides these atomistic models Stevens and coworkers modeled polymeric networks using a coarse-grained representation with dynamical cross-linking procedure [67-69]. They investigated the effects of the cross-linker functionality, the network connectivity on the mechanical properties and the influence of bond density on interfacial fracture. Their work has shown that a coarse-grained representation enables simulation of networked systems at longer time and length scales while capturing the experimentally observed essential mechanical features.

Inspired by the success of using ionic interactions in the healing of projectile puncture, here we seek a parallel means of adding self-healing character to cross-linked polymers. Specifically, we investigate mechanical properties in a polymer network with ion pairs embedded throughout using a generic coarse-grained representation of the system. We explore the possibility of enhancing toughness by ionic links and the potential underlying mechanisms using molecular dynamics simulations. We have paid attention also to the effect of the rate of deformation applied to the network.

This article is organized as follows. Section 2 describes the details of the model and the simulation protocol. The results of our study are presented in Sec. 3. Particularly, the stress-strain curves of the standard and the ionic networks upon tensile and shear modes of deformations were presented. The possible mechanisms behind the results were discussed in Sec. 4. The conclusions of this work are given in Sec. 5 followed by the appropriate acknowledgments.

Model and Simulation Protocol

The cross-linked system was represented using the bead-spring model based closely on the works of Stevens and coworkers [67-69]. We briefly introduce the bonded and non-bonded potentials used. The interactions between the beads were described using 6-12 Lennard-Jones (LJ) potential (Equation (1)) with a 2.5 d cutoff.

49

$$U_{LJ}(r) = 4u_0 \left[\left(\frac{d}{r} \right)^{12} - \left(\frac{d}{r} \right)^6 \right] \tag{1}$$

where u_0 is the LJ energy, d is the LJ diameter and r is the distance between two interacting beads. Both u_0 and d were taken as unity.

The beads are bonded via a quartic bond potential (Equation (2)).

$$U_q(r) = \begin{cases} k(y-b_1)(y-b_2)y^2 + U_0, & r < r_c \\ U_0, & r > r_c \end{cases} \tag{2}$$

where $y = r - \Delta r$ that shifts the quartic center from the origin and the parameters as adopted directly from the study by Stevens et al. [67] are k = 1434.3 u_0/d^4, b_1 = -0.759 d, b_2 = 0.0, $\Delta r = r_c =$ 1.5 d and U_0 = 67.223 u_0. The bond potential is smoothly cutoff at r_c. At distances larger than r_c the bond potential is turned off that leaves only LJ term remaining. The bond breakage is irreversible. The bond potential parameters result in maximum bonding force of 156.7 u_0/d compared to maximum LJ force of 2.4 u_0/d.

Coulombic interactions for pairs of ionic beads were computed with a cutoff of also 2.5 d.

$$U_{Coul}(r) = \frac{1}{4\pi\varepsilon_0} \frac{q_i q_j}{r} \tag{3}$$

where q_i is the charge on bead i, ε_0 is dielectric constant. As this is a coarse grained model with each bead representing many atoms, the size of a bead is much larger than atoms. Therefore, when the charges are placed at the center of large beads, ionic bonds (i.e. two oppositely charged neighboring beads) are separated by large distances. Thus, the Coulombic force between two neighboring beads falls short of a realistic ionic interaction. In order to bring the ionic interaction force to a more realistic quantity we set the dielectric constant (ε_0) to 0.02. This dielectric constant was selected in order to situate the ratio of the maximum quartic bonding force to ionic interaction force at about 50. This ratio is simply an estimate value that relates the strength of an typical covalent bond to an ionic bond. In fact, at r = 1.12 d the ionic force is 3.17 u_0/d versus 156.7 u_0/d (i.e. ratio of 49.4).

The MD simulations were performed using LAMMPS (Large-scale Atomic/Molecular Massively Parallel Simulator) [70]. The equations of motion were integrated using the Verlet algorithm [42] with a time step of 0.05 τ, where τ is the LJ time unit. The long-range Coulombic interactions beyond the cutoff (reciprocal sum) were calculated using the particle-particle

particle-mesh Ewald (PPPM) solver with a precision value of 1.0×10^{-3}. Both temperature and pressure were controlled using Nosé-Hoover formalism with a damping constant of 0.1τ.

The initial simulation box consisted of small chains with two and three beads that were sandwiched between two rigid layers of beads. The chains with three beads contained one bead designated as the cross-linker bead for subsequent cross-linking process. The layers were made of (111) plane of face-centered cubic (FCC) lattice structure with lattice spacing of 1.2. They interact with all beads except themselves. The system consisted of a total number of 103,344 beads of *chain*, *cross-linker* and *layer* type, where the ratio of the two- and three-bead chains was determined by stoichiometry. The liquid mixture was first equilibrated in canonical ensemble (NVT) at 1.0 reduced temperature unit (T^*), followed by the density equilibration in NPT (isobaric-isothermal) ensemble. The pressure was imposed anisotropically in *z*-axis while no pressure scaling was employed in *x* and *y* directions.

The liquid mixture was dynamically cross-linked after the equilibration. Briefly, a varying distance criterion was used first to determine the candidate pairs (i.e. a bead and a *cross-linker* bead with a functionality of four) which then were sequentially cross-linked. The selected separation distance ranged from 1.1 *d* at the first step until 1.35 *d* at the final cross-linking step. Each step consisted of: 1. determination of pairs, 2. creation of bonds and 3. equilibration of the system. The cross-linking (first to beads in the layers and then in the bulk) was carried on for a total of 40 and 60 steps, respectively. The number of steps for the first cross-linking stage was adjusted to create adequate cross-linking density on the layers so that cohesive failure was promoted. The second cross-linking stage was continued until a sufficient degree of cross-linking was achieved in the bulk. Near the end of each cross-linking stage, only a few or no additional cross-linking occurred. As a result, about 60,000 cross-linking bonds were created with nearly 5,000 of them formed to the beads in the rigid layers, leading to 98% degree of cross-linking. After equilibration of the network at 1.0 T^*, the harmonic bond potential used hitherto was replaced with the quartic potential. Subsequently, the system was slowly cooled down (at a rate of 1.4×10^{-5} T^* per MD step) to 0.3 T^*, which is well below the estimated glass transition temperature.

Ionic bonds were incorporated into the fully cross-linked network subsequent to its equilibration. The bond between a pair of randomly selected consecutive beads was removed to create ionic bonds. In the case of an ionic network, these beads were assigned opposite charges

to create ionic bonds while for a standard network they were left unchanged. Using this approach, we created a new network with the same network density (82%) as non-ionic one but with ionic bonds incorporated within. The fact that we used pairs of beads bonded to each other to create ionic pairs is actually expected to reflect a molecular arrangement close to an actual system. Namely, one would anticipate in the actual synthesis of a polymeric network that the monomers with opposite charges would be at close proximity as the cross-linking reactions take place.

Two forms of deformation (tensile and shear) were applied in a quasi-equilibrium fashion. In tensile mode, the upper layer was displaced along the *z*-direction with a selected speed over an increment of 0.5 *d*. Subsequently, the simulation was run at the new position for the same number of simulation steps needed for the displacement. The data for the calculation of stress-strain curves were collected at this stage. The effective deformation rate, therefore, is half of the selected displacement speed. The two selected speeds 0.5×10^{-1} and 0.5×10^{-2} *d*/τ resulted in strain rates of 0.6×10^{-3} and 0.6×10^{-4} 1/τ, respectively. In the case of shear deformation the upper layer was displaced in the *x*-direction.

Results

We begin our analyses with a careful look into the microstructure of the ionic network using a set of radial distribution functions (g(*r*)) shown in Figure 25. g(*r*)*chain-chain* exhibits an initial sharp peak located at 0.95 and a broader peak at 1.07 *d* corresponding to the bonded and the non-bonded interactions among the beads of *chain* type, respectively. In other words, the quartic bond potential with the parameters used in this study shows a minimum in the potential energy at 0.93 *d* that agrees with the position of the initial peak, while the energy minimum in Lennard-Jones potential for the non-bonded interactions is at 1.12 *d* in line with the second peak. The remainder of the g(*r*)*chain-chain* has shallower and dying out peaks that is reminiscent of liquids. g(*r*)*xlinker-xlinker* is very similar to g(*r*)*chain-chain* suggesting that the *cross-linker* beads are uniformly distributed in the network. However, the absence of a sharp peak near 0.93 *d* signifies that cross-linkers are not bonded to one another. The sharp spike-like peaks in g(*r*)*xlinker-layer* indicate a layer by layer positioning of *cross-linker* beads near the layers. The first peak is a result of *cross-linkers* directly bonded to the layers, while the second (~1.6 *d*) and third (~2.0 *d*) peaks are due to the *cross-linkers* that are separated from layers by one and two layers of beads, respectively. The intensity of these peaks diminishes rapidly with *r*. This type of arrangement

shows that the network has a fairly ordered structure near the layers ($r <$ ~5 d) that becomes amorphous-like away from the layers. The relative positioning of ionic pairs are presented by g(r)$_{ion-ion}$. There is a single and dominant peak at 0.97 d pointing to the fact that they were created from pairs of beads which were initially bonded (i.e. pairs of *cross-linker* and *chain*).

After this brief examination of the microstructure we will now investigate the material responses to different forms of deformation for both control and ionic networks starting with the tensile deformation in Figure 26 (lower panel). There is a clear peak at 0.1 seen for both networks corresponding to the yield behavior. The yield stress originates from the LJ interactions. For this reason, the yield peak appears to be very distinct due to the fact that the networks have a lower degree of cross-linking than a fully cross-linked system. The yield point, which is effectively independent of the degree of cross-linking, becomes larger than the rest of the stress-strain curve since the degree of cross-linking was lowered to 82%. Note also that the equilibrium distance of the LJ potential is at 1.12 d, while the maximum force occurs at 1.25 d. Therefore, it takes a strain of about 0.1 to bring the network from the equilibrium LJ separation to a separation of the maximum resistance.

In the standard network, subsequent to the yield stress there is plateau region that lasts until about $\varepsilon = 1.0$. During this period the strands connecting two cross-linkers are being extended while bonds remain mostly intact as described by Stevens [67]. The bonds start breaking appreciably only after about $\varepsilon = 1.2$ (see upper panel in Figure 26) and the network fails ultimately at about $\varepsilon = 2.0$. The ionic network exhibits a similar behavior to the standard network, but with some imperative differences. First, after the yield behavior the values of stress do not drop as extensively as the standard network. The stress-strain curve remains above that of the standard network indicating that the addition of ionic bonds improves the toughness (i.e. the area under this curve). Another key result is that the ionic network requires nearly twice as many bonds to be broken to fail compared to the standard network. We also observe that the ultimate failure does not occur abruptly due to lower degree of cross-linking and limited system size.

Snapshots of the network under tensile deformation at five consecutive strains are presented in Figure 27 to aid visualizing the deformation in tensile mode. At $\varepsilon = 0.5$, there are voids formed in the network. They actually emerge as strain passes through the yield point. Their formation does not require breaking of bonds since they are already present but in compacted form. Moreover, their presence indicates that the cross-linking is not entirely homogenous: there

are regions of highly dense degree of cross-linking and those of lesser amount of cross-links. They basically act as defects that initiate cracks. At $\varepsilon = 1.0$, the voids grow further and the surrounding areas approach their limits of the stress they can carry without breaking of bonds. Later, at $\varepsilon = 1.5$, the stretching strands that bear the load become more visible. At this stage, there is a considerable degree of bond breaking and the network starts to break into two pieces. Finally, at $\varepsilon = 2.0$, the network has nearly failed with only a single strand holding the newly created interfaces.

The response to deformation in shear mode is presented in Figure 28. The initial rapid rise of stress and the subsequent slowing down at $\varepsilon = 0.1$ is due to the yield behavior. The magnitude of the yield stress for the standard network is 0.07 u_0/d^3 which is in agreement with 0.08 u_0/d^3 found in the earlier study [67]. The yield stress in this deformation mode stems from the frictional resistance between two sliding surfaces interacting via LJ beads. After the yield point, stress continues to rise first, at a lower rate, and later ($\varepsilon > \sim 1.2$) at a higher rate until it reaches the maximum point (i.e. where the ultimate failure occurs). Note that the bond breaking continues even after the maximum point, because the failure results in a rough interface. This interface is smoothened while being sheared, thus bond breaking continues until two sufficiently smooth surfaces are attained. Subsequently, the shearing would constitute shearing of two flat surfaces interacting via LJ interactions similar to the case at the yield point. Therefore, if simulation was pursued further the stress would eventually level off at about the yield stress.

In the earlier studies [67, 68] the maximum point was followed by a sudden drop in stress. This drop is more gradual in our study possibly because of the lower degree of cross-linking since densely cross-linked networks fail more abruptly. The comparison of networks shows that stress increases in ionic network more rapidly than the standard network and maintains its elevated level until the point of maximum stress. Similar to what was found in the deformation in tensile mode, the incorporation of ionic pairs appears to raise the shear stress thus generating a tougher network. However, after the maximum stress is reached both curves become nearly overlapping.

The deformation in shear mode is illustrated in Figure 29 using six snapshots taken at ascending strain values. At $\varepsilon = 0.7$, stripes are stretched to sigmoidal-like shape. As the network is stretched further at $\varepsilon = 1.3$, 2.0 and 2.6 they get straighter and thinner showing that strands are

extended at or beyond their limits before breaking. Finally, at $\varepsilon = 3.3$, close observation reveals that the location of interfacial failure is near the middle of the lower half of the Figure 29 (e).

Discussion

We found consistently in both tensile and shear modes of deformation that the ionic network requires a larger number of bonds to be broken before the ultimate failure occurs. In order to understand the origins of this behavior, we first determined the positions of the failing bonds. These bonds, as identified in Figure 30, indicate the location of the interfacial failure. For example, the clustering of these broken bonds in the lower portion of the Figure 30 (a) points to the location of failure as confirmed by Fig. 3 for the deformation of the standard network in tensile mode. Figure 30 (c) shows that, in the case of ionic network, these bonds are present not only in the location of the failure but also in the surrounding area by a larger quantity than the control network (Figure 30 (a)). This result is even clearer in shear mode (Figure 30 (b) vs. (d)).

We infer that the integration of ionic pairs bring about a network that can distribute the stress more uniformly, which in turn results in improved mechanical properties. In order to gain insight into how the stress is distributed more uniformly we looked at the growth of voids that form with tensile deformation. It is an important phenomenon because the strands surrounding voids are where the stresses concentrate. The snapshots of voids are shown in Figure 31 at varying strains. At the yield point ($\varepsilon = 0.1$), voids are visible in their early form. They appear to be more randomly distributed initially in the standard than the ionic network, while at strains $\varepsilon >$ 1.0 they are equally randomly distributed. The variation in their distribution is not expected to affect the mechanical properties significantly, because the difference in randomness is seen only until bond breaking starts. However, it is notable to observe that the sizes of voids are smaller in the ionic network compared to the standard network at any strain. The smaller void sizes in the ionic network shows that the load can be more uniformly distributed throughout the network, hence overall mechanical properties are improved, in line with our analysis of distribution of broken bonds.

We had observed earlier that the shear stress is enhanced up to the point of the interfacial failure (Figurd 28). After this point, stresses became indistinguishable between the two types of networks. Unlike this observation, when a lower deformation rate (by an order of magnitude) is applied (see Figure 7), the ionic network continues to bear a higher load even after the point of the maximum stress. Knowing that the two experiments differ only by the deformation rate and

55

that the networks differ only by the presence of ionic pairs, this result indicates that it is a consequence of the rate dependence of ionic pairs. A plausible explanation is that the ionic pairs that deform as a result of shearing are able to re-form only when the system is deformed with a low strain rate so that the strands Figure 32 have enough time to relax. We infer also that this time dependency refers to the presence of a self-healing mechanism that restores the strength of the network.

Concluding Remarks

We presented results for a coarse-grained model of cross-linked networks with and without ionic bonds incorporated. The MD simulations of the deformation of the networks in tensile and shear mode showed that the model has captured the fundamental mechanical features such as the yield behavior and the strain hardening.

One is bound by the length scale that can be practically modeled, as an inherent limitation of molecular level simulations. This constraint reflected itself for the current system in two ways. First, how the stress is transferred from the solid layers to the network should be a function of the distance between the upper and lower layers. The interfacial failures that occur in the vicinity of the layers, rather than in the middle section in all four cases may be a consequence of the stress build up in this region. Secondly, the network can be only as heterogeneous as the system size. In fact, the main reason why the system fails only after very high strains ($\varepsilon > 2$) is that the crack initiation can occur only after strands are extended significantly. In a real material there would be *a heterogeneous cross-linking* (i.e. broad distribution of degree of freedom of strands to stretch). When the deformation is applied, the strands with a low degree of freedom to stretch will be stressed the most and break first. These regions where such constrained strands concentrate will act as defects that initiate cracks before the rest could collectively stretch. From this point of view, the current model appears to represent an ideal network compared to a real one. Another interpretation is that the model is capturing the deformation behavior at or near the crack tip as suggested previously [67-69].

The primary outcome of this work is the finding that the integration of ionic pairs elevated the level of stress that the network can withstand over a wide range of strain values in both tensile and shear mode of deformation. This implies that ionic pairs create a stronger and tougher network compared to the control network. We identified two plausible mechanisms through which the ionic pairs became effective. They were able to reform after being displaced

due to deformation and they enabled a more uniform distribution of the stress throughout the network.

In future work, we plan to investigate the effects of the cross-link density, content of ionic pairs and the interplay between them.
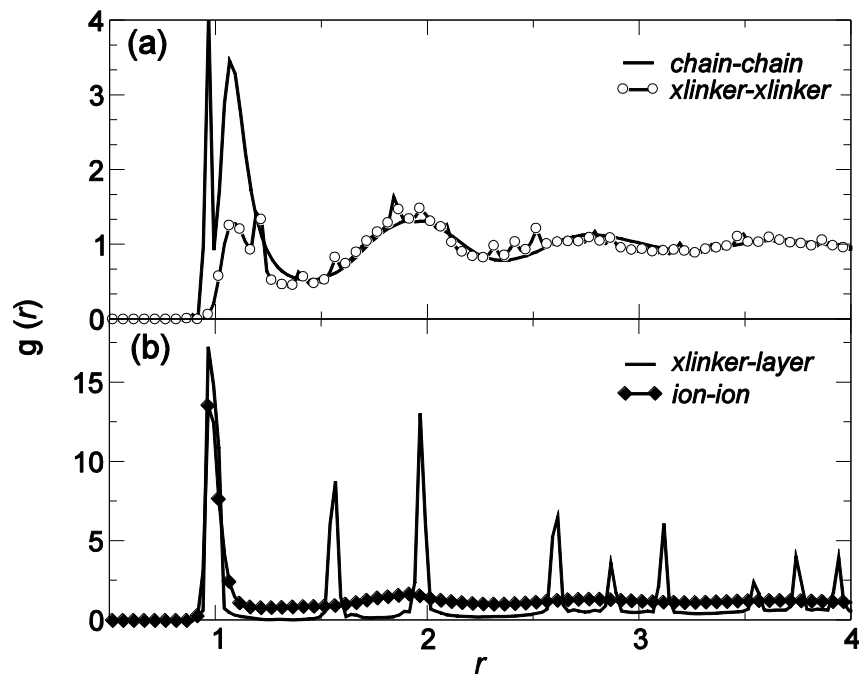
Figure 25. Radial distribution functions of pairs of (a) *chain-chain* and *xlinker-xlinker* and (b) *ion-ion* and *layer-xlinker* type beads.
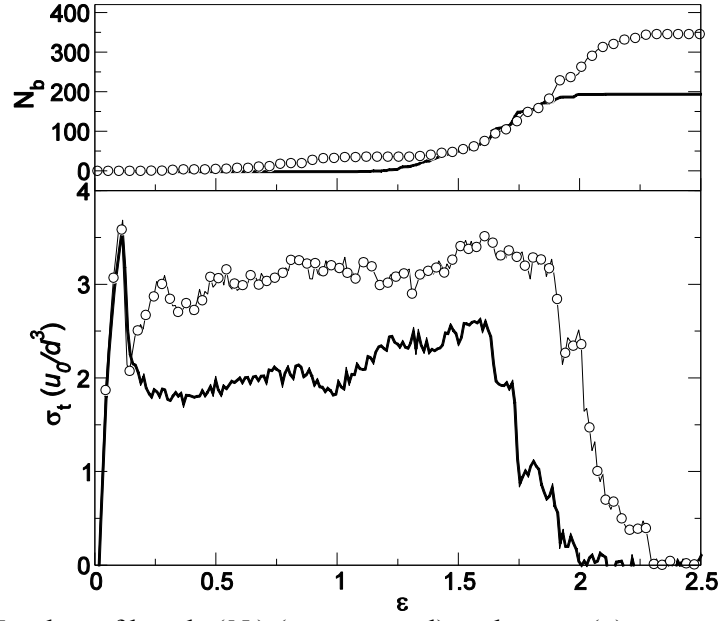
Figure 26. Number of bonds (N_b) (upper panel) and stress (σ) versus strain (ε) behavior upon tensile deformation at strain rate of 0.6×10^{-3} $1/\tau$. Standard network (line) and ionic network (circles).
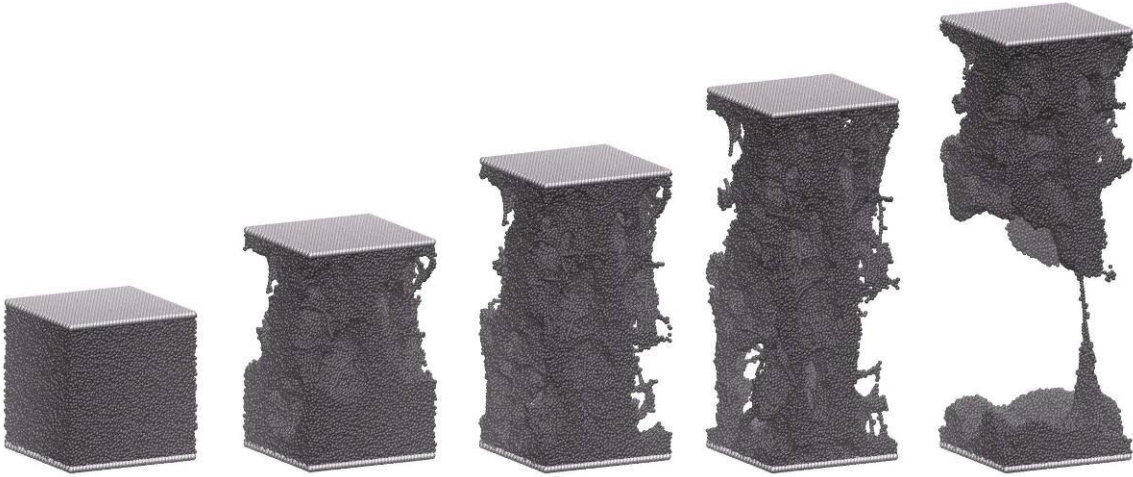
Figure 27. Views of the network during deformation in tensile mode at $\varepsilon = 0.0$, 0.5, 1.0, 1.5 and 2.0.
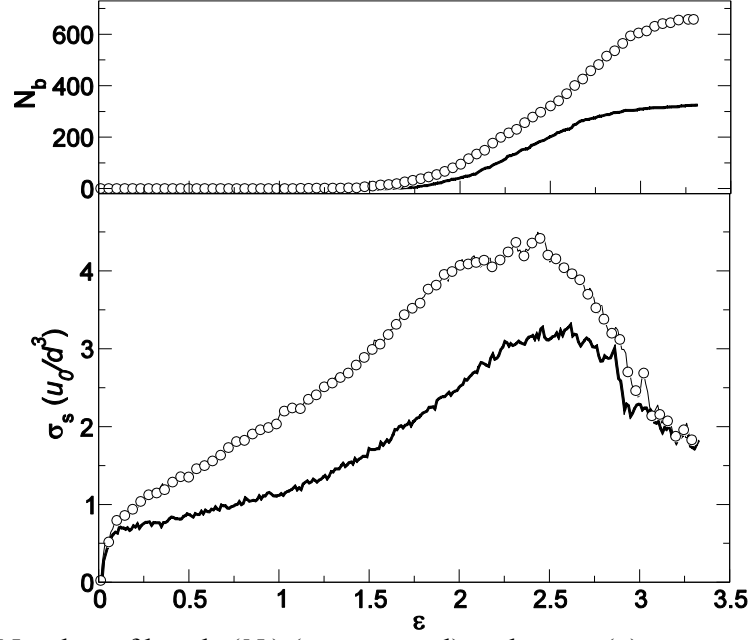
Figure 28. Number of bonds (N_b) (upper panel) and stress (σ) versus strain (ε) behavior upon shear deformation at strain rate of 0.6×10^{-3} $1/\tau$. Standard network (line) and ionic network (circles).
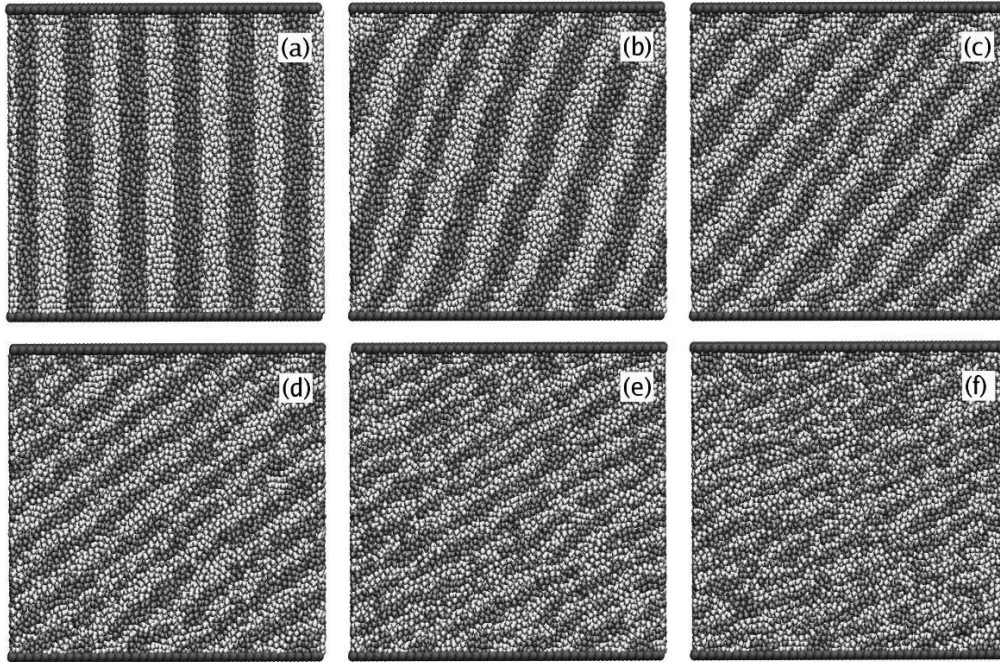
Figure 29. Views of the network through x-z plane during shear deformation at strain values of (a) 0.0, (b) 0.7, (c) 1.3, (d) 2.0, (e) 2.6, and (f) 3.3. The beads are colored in stripes to help visualize the shearing.

59
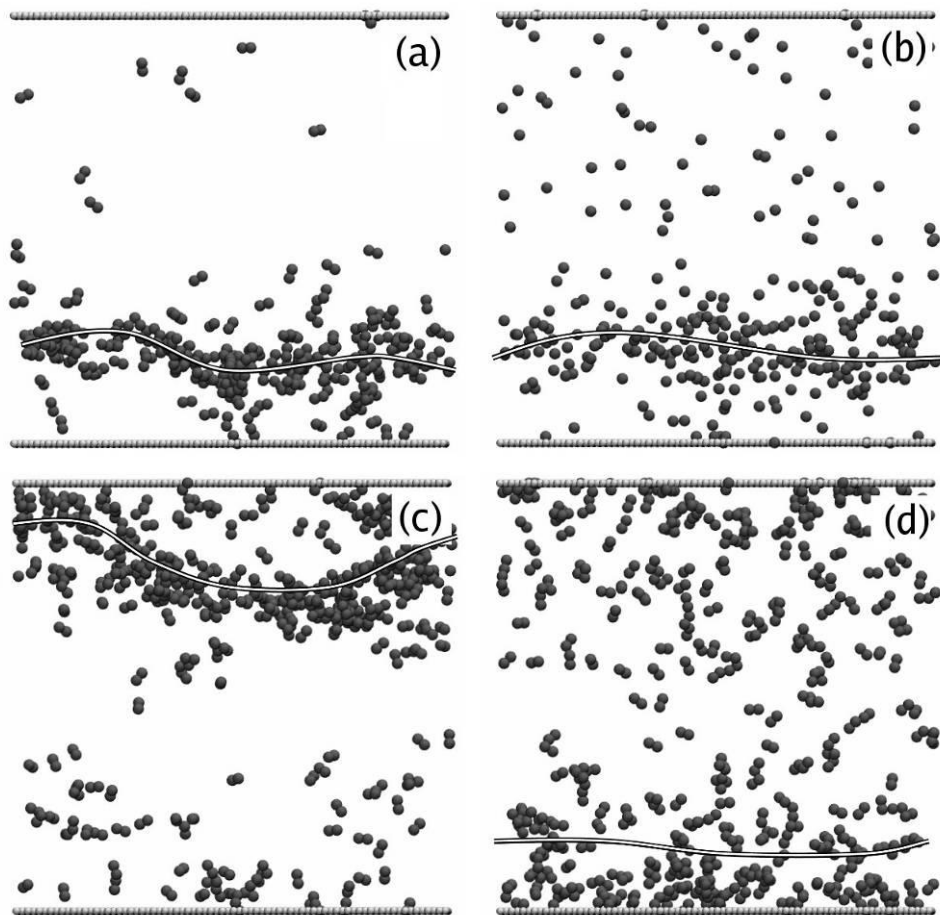
Figure 30. Views (through *x-z* plane) of pairs of beads forming bonds that eventually brake after applying deformation. Upper half shows views for the control network after deformation in (a) tensile and (b) shear mode. Similarly, lower half shows views for the ionic network after deformation in (c) tensile and (d) shear mode. The lines highlight approximate locations of ultimate interfacial failure.
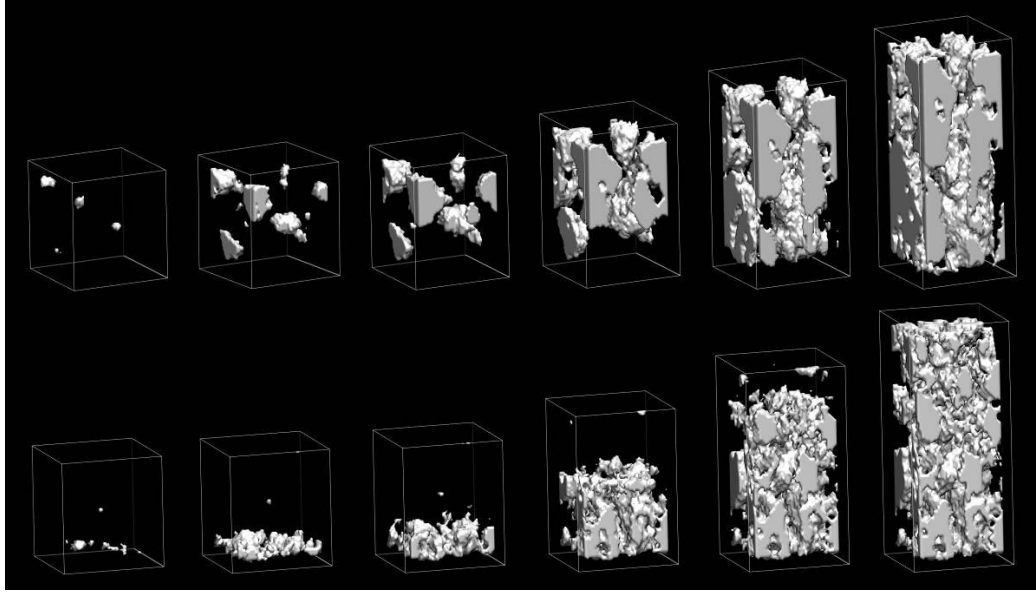
Figure 31. Snapshots of the voids as they develop during tensile deformation in the standard (upper panel) and the ionic (lower panel) networks. Strains at which snapshots were generated are (from left to right): 0.1, 0.15, 0.25, 0.5, 1.0 and 1.5.
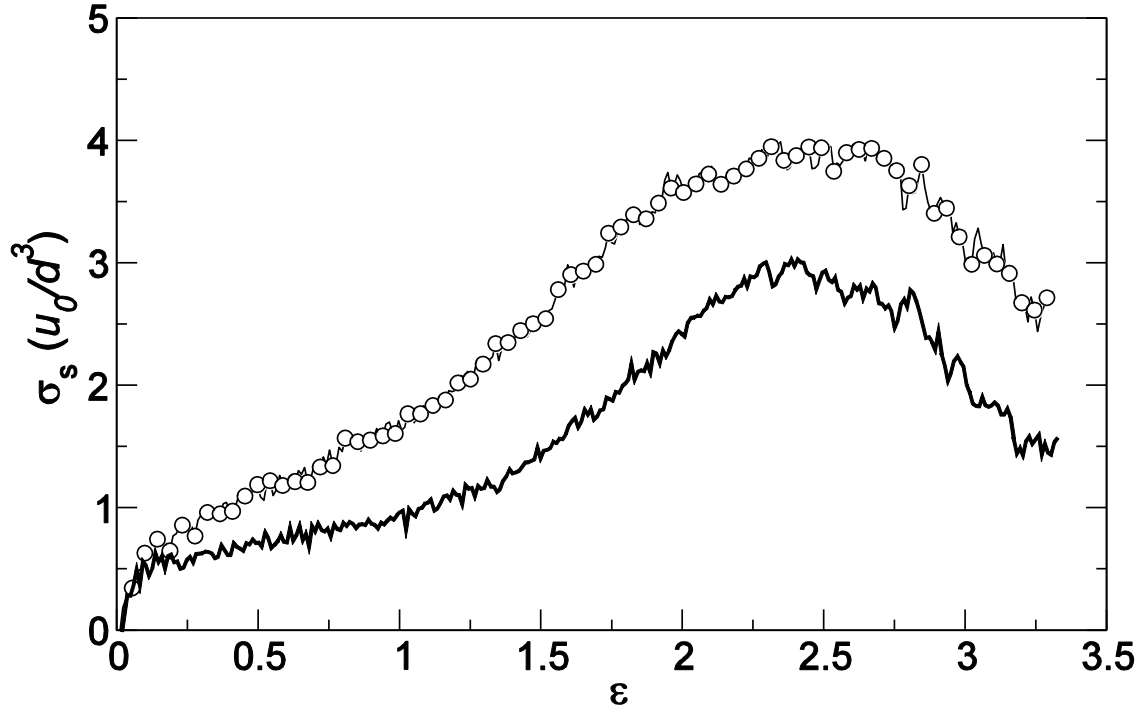
Figure 32. Stress (σ) versus strain (ε) behavior upon shear deformation at strain rate of 0.6×10^{-4} $1/\tau$. Standard network (line) and ionic network (circles).

2.4   Mechanisms of Gecko Adhesion

Gecko's exceptional ability in climbing up smooth vertical surfaces has intrigued many scientists leading to a detailed investigation of the mechanisms of gecko's adhesion. Microscopy has shown that a gecko's foot has a hierarchy of structures: nearly five hundred thousand 30-130 μm long setae in the foot branching into hundreds of projections terminating in 0.2-0.5 μm spatula-shaped structures (see Figure 33, left). While the strong adhesion ability is attributed to this hierarchical structure and the rapidly releasing ability to the anisotropy in the spatula, there is no fundamental understanding of the basic adhesion-deadhesion mechanism. The knowledge of this mechanism would have important implications in designing responsive adhesive biomimetic systems. We plan modeling the unique structure of the spatula as a networked system in a coarse-grained representation of the repeating unit (Figure 33, right). We plan to compare the simulation results to the experimental measurements of the directional adhesion of model systems and to bring insight into the fundamentals of the process.

Thus far, we used a two-dimensional coarse-grained approach to model a cross-linked parallelepiped body with a 50° tilt. This shape is intended to mimic the type of anisotropy that appears to be the underlying mechanism in gecko's adhesion-release ability to surfaces. Computer simulations of detachment experiments at varying detachment directions were carried out. Early results have shown a qualitative agreement with experimental measurements of directional adhesion for a similar system by Guduru at Brown University.
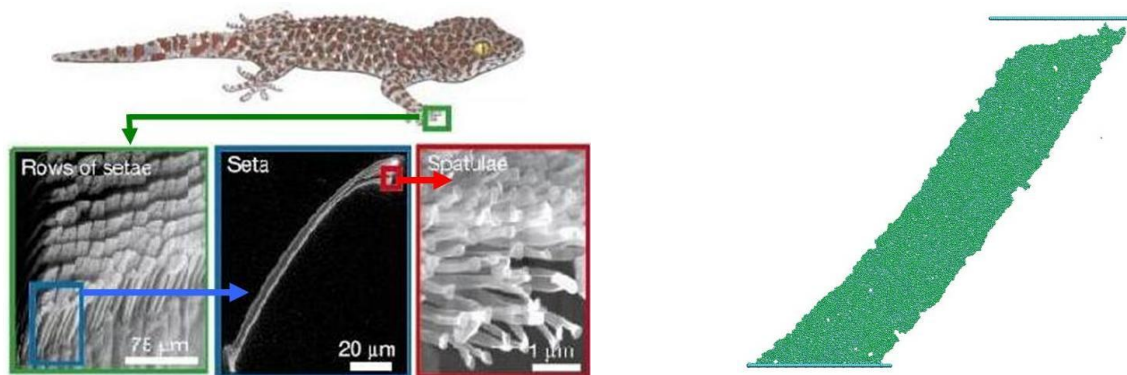
Figure 33. (Left) Hierarchical structure of gecko's foot. (Right) A model of tilted pillar in coarse-grained representation.

REFERENCES

(1)   Adams, D. M.; Brus, L.; Chidsey, C. E. D.; Creager, S.; Creutz, C.; Kagan, C. R.; Kamat, P. V.; Lieberman, M.; Lindsay, S.; Marcus, R. A.; Metzger, R. M.; Michel-Beyerle, M. E.; Miller, J. R.; Newton, M. D.; Rolison, D. R.; Sankey, O.; Schanze, K. S.; Yardley, J.; Zhu, X., *J. Phys. Chem. B* **2003,** *107*, 6668.

(2)   Gooding, J. J.; Mearns, F.; Yang, W.; Liu, J., *Electroanalysis* **2003,** *15*, 81.

(3)   Chaki, N. K.; Vijayamohanan, K., *Biosens. Bioelectron.* **2002,** *17*, 1.

(4)   Xia, Y.; Whitesides, G. M., *Angew. Chem. Int. Ed.* **1998,** *37*, 550.

(5)   Lio, A.; Charych, D. H.; Salmeron, M., *J. Phys. Chem. B* **1997,** *101*, 3800.

(6)   Scherer, J.; Vogt, M. R.; Magnussen, O. M.; Behm, R. J., *Langmuir* **1997,** *13*, 7045.

(7)   Nitzan, A.; Ratner, M. A., *Science* **2003,** *300*, 1384.

(8)   Fenter, P.; Eisenberger, P.; Liang, K. S., *Phys. Rev. Lett.* **1993,** *70*, 2447.

(9)   Mar, W.; Klein, M. L., *Langmuir* **1994,** *10*, 9.

(10)   Ulman, A., *Chem. Rev.* **1996,** *96*, 1533.

(11)   Schreiber, F., *Prog. Surf. Sci.* **2000,** *65*, 151.

(12)   Love, J. C.; Estroff, L. A.; Kriebel, J. K.; Nuzzo, R. G.; Whitesides, G. M., *Chem. Rev.* **2005** *105*, 1103.

(13)   Vericat, C.; Vela, M. E.; Salvarezza, R. C., *Phys. Chem. Chem. Phys.* **2005,** *7*, 3258.

(14)   Vericat, C.; Vela, M. E.; Benitez, G. A.; Gago, J. A. M.; Torrelles, X.; Salvarezza, R. C., *J. Phys.: Condens. Matter* **2006,** *18*, R867.

(15)   Kornilovitch, P. E.; Bratkovsky, A. M., *Phys. Rev. B* **2001,** *64*, 195413.

(16)   Krstic, P. S.; Dean, D. J.; Zhang, X.-G.; Keffer, D.; Leng, Y. S.; Cummings, P. T.; Wells, J. C., *Comput. Mater. Sci.* **2003,** *28*, 321.

(17)   Hong, S.; Reifenberger, R.; Tian, W.; Datta, S.; Henderson, J. I.; Kubiak, C. P., *Superlattices Microstruct.* **2000,** *28*, 289.

(18)   Jung, H. H.; Won, Y. D.; Shin, S.; Kim, K., *Langmuir* **1999,** *15*, 1147.

(19)   Kim, Y.-H.; Jang, S. S.; Goddard III, W. A., *J. Chem. Phys.* **2005,** *122*, 244703.

(20)   Collard, D. M.; Fox, M. A., *Langmuir* **1991,** *7*, 1192.

(21)   Schlenoff, J. B.; Li, M.; Ly, H., *J. Am. Chem. Soc.* **1995,** *117*, 12528.

(22)   Bumm, L. A.; Arnold, J. J.; Cygan, M. T.; Dunbar, T. D.; Burgin, T. P.; Jones, L., II; Allara, D. L.; Tour, J. M.; Weiss, P. S., *Science* **1996,** *271*, 1705.

(23)   Ramachandran, G. K.; Hopson, T. J.; Rawlett, A. M.; Nagahara, L. A.; Primak, A.; Lindsay, S. M., *Science* **2003,** *300*, 1413.

(24)   Howell, S.; Kuila, D.; Kasibhatla, B.; Kubiak, C. P.; Janes, D.; Reifenberger, R., *Langmuir* **2002,** *18*, 5120.

(25)   Vandamme, N.; Schouteden, K.; Snauwaert, J.; Lievens, P.; Van Haesendonck, C., *Surf. Sci.* **2006,** *600* 2894.

(26)   Barriet, D.; Yam, C. M.; Shmakova, O. E.; Jamison, A. C.; Lee, T. R., *Langmuir* **2007,** *23*, 8866.

(27)   Abduaini, A.; Kera, S.; Aoki, M.; Okudaira, K. K.; Ueno, N.; Harada, Y., *J. Electron Spectrosc. Relat. Phenom.* **1998,** *88-91*, 849.

(28)   Pugmire, D. L.; Tarlov, M. J.; van Zee, R. D.; Naciri, J., *Langmuir* **2003,** *19*, 3720.

(29)   Wang, J.; Wolf, R. M.; Caldwell, J. W.; Kollman, P. A.; Case, D. A., *J. Comput. Chem.* **2004,** *25*, 1157.

(30)   Dirama, T. E. Ph.D. thesis, the University of Akron, Akron, OH, 2005.

(31)   Mayo, S. L.; Olafson, B. D.; Goddard, W. A., *J. Phys. Chem.* **1990,** *94*, 8897.

(32)   Jang, S. S.; Jang, Y. H.; Kim, Y. H.; Goddard, W. A.; Flood, A. H.; Laursen, B. W.; Tseng, H. R.; Stoddart, J. F.; Jeppesen, J. O.; Choi, J. W.; Steuerman, D. W.; DeIonno, E.; Heath, J. R., *J. Am. Chem. Soc.* **2005,** *127*, 1563.

(33)   Lavrich, D. J.; Wetterer, S. M.; Bernasek, S. L.; Scoles, G., *J. Phys. Chem. B* **1998,** *102*, 3456.

(34)   Rappe, A. K.; Casewit, C. J.; Colwell, K. S.; Goddard, W. A.; Skiff, W. M., *J. Am. Chem. Soc.* **1992,** *114*, 10024.

(35)   Dirama, T. E.; Neely, S. V.; Johnson, J. A., unpublished.

(36)   Fenter, P.; Schreiber, F.; Zhou, L.; Eisenberger, P.; Forrest, S. R., *Phys. Rev. B* **1997,** *56*, 3046.

(37)   Case, D. A.; Darden, T. A.; Cheatham III, T. E.; Simmerling, C. L.; Wang, J.; Duke, R. E.; Luo, R.; Merz, K. M.; Wang, B.; Pearlman, D. A.; Crowley, M.; Brozell, S.; Tsui, V.; Gohlke, H.; Mongan, J.; Hornak, V.; Cui, G.; Beroza, P.; Schafmeister, C.; Caldwell, J. W.; Ross, W. S.; Kollman, P. A. *AMBER 8*, University of California: San Francisco, 2004.

(38)   Jakalian, A.; Bush, B. L.; Jack, D. B.; Bayly, C. I., *J. Comput. Chem.* **2000,** *21*, 132.

(39)   Tao, Y. T.; Wu, C. C.; Eu, J. Y.; Lin, W. L.; Wu, K. C.; Chen, C. H., *Langmuir* **1997,** *13*, 4018.

(40)   Plimpton, S., *J. Comput. Phys.* **1995,** *117*, 1.

(41)   Hockney, R. W.; Eastwood, J. W., *Computer Simulation Using Particles*. McGraw-Hill International Book Co: New York, 1981.

(42)   Verlet, L., *Phys. Rev.* **1967,** *159*, 98.

(43)   Nosé, S., *J. Chem. Phys.* **1984,** *81*, 511.

(44)   Hoover, W. G., *Phys. Rev. A* **1985,** *31*, 1695.

(45)   Leung, T. Y. B.; Schwartz, B.; Scoles, G.; Schreiber, F.; Ulman, A., *Surf. Sci.* **2000,** *458*, 34.

(46)   Yourdshahyan, Y.; Zhang, H. K.; Rappe, A. M., *Phys. Rev. B* **2001,** *63*, 081405.

(47)   Dhirani, A. A.; Zehner, R. W.; Hsung, R. P.; Guyot-Sionnest, P.; Sita, L. R., *J. Am. Chem. Soc.* **1996,** *118*, 3319.

(48)   Butt, H. J.; Cappella, B.; Kappl, M., *Surface Science Reports* **2005,** *59*, 1.

(49)   Ahimou, F.; Denis, F. A.; Touhami, A.; Dufrene, Y. F., *Langmuir* **2002,** *18*, 9937.

(50)   He, H. X.; Huang, W.; Zhang, H.; Li, Q. G.; Li, S. F. Y.; Liu, Z. F., *Langmuir* **2000,** *16*, 517.

(51)   Schonherr, H.; Chechik, V.; Stirling, C. J. M.; Vancso, G. J., *J. Am. Chem. Soc.* **2000,** *122*, 3679.

(52)   van der Vegte, E. W.; Hadziioannou, G., *Langmuir* **1997,** *13*, 4357.

(53)   Vezenov, D.; Noy, A.; Rozsnyai, L. F.; Lieber, C. M., *J. Am. Chem. Soc.* **1997,** *119*, 2006.

(54)   Chen, Y. Z., *Phys. Rev. E* **1999,** *60*, 5938.

(55)   Dirama, T. E.; Johnson, J. A., *Langmuir* **2007,** *23*, 12208.

(56)   Butt, H.-J.; Franz, V., *Phys. Rev. E* **2002,** *66*, 031601.

(57)   Paramonov, P. B.; Lyuksyutov, S. F.; Mayevska, O. V.; Reagan, M. A.; Umemura, K.; Tobari, H.; Hara, M.; Vaia, R. A.; Juhl, S., *Langmuir* **2006,** *22*, 6555.

(58)   Balazs, A. C., *Materials Today* **2007,** *10*, 18.

(59)   Kessler, M. R., *Proceedings of the Institution of Mechanical Engineers, Part G: Journal of Aerospace Engineering* **2007,** *221*, 479.

(60)   Eisenberg, A.; Hird, B.; Moore, R. B., *Macromolecules* **1990,** *23*, 4098.

(61)   Tadano, K.; Hirasawa, E.; Yamamoto, H.; Yano, S., *Macromolecules* **1989,** *22*, 226.

(62)   Din, X. D.; Michaelides, E. E., *AIChE J.* **1998,** *44*, 35.

(63)   Vishnyakov, A.; Neimark, A. V., *J. Phys. Chem. B* **2000,** *104*, 4471.

(64)   Elliott, J. A.; Hanna, S.; S., E. A. M.; Cooley, G. E., *Phys. Chem. Chem. Phys.* **1999,** *1*, 4855.

(65)   Yarovsky, I.; Evans, E., *Polymer* **2002,** *43*, 963.

(66)   Heine, D. R.; Grest, G. S.; Lorenz, C. D.; Tsige, M.; Stevens, M. J., *Macromolecules* **2004,** *37*, 3857.

(67)   Stevens, M. J., *Macromolecules* **2001,** *34*, 2710.

(68)   Tsige, M.; Lorenz, C. D.; Stevens, M. J., *Macromolecules* **2004,** *37*, 8466.

(69)   Tsige, M.; Stevens, M. J., *Macromolecules* **2004,** *37*, 630.

(70)   Plimpton, S., *J. Comput. Phys.* **1995,** *117*, 1.

TIMELINE OF TECHICAL PROGRESS

December-2005

In the past month I have reviewed the current literature on the newly assigned project of developing ice-phobic materials. I have worked on introducing the idea of using the anti-freeze proteins for developing ice-phobic materials. It has been recently discovered that antifreeze proteins, found in organisms that can survive in extremely cold environments (e.g. Antarctic fish), disrupt ice growth in a non-colligative manner. These proteins may directly be utilized as ice inhibitors or the knowledge of how they function can be used for designing novel coating systems. I am planning on modeling the coating surface- anti-freeze protein interactions. This computational effort may potentially initiate an innovative path towards developing ice-phobic materials.

I have also researched computer hardware and software that will be required for the modeling and simulation effort. Particularly, I have configured and collected quotes for a workstation and a Beowulf cluster. As configuring Beowulf clusters require a great deal of

knowledge in concepts such as parallel computing, message passing interface, network interconnect etc. I have spent considerable amount of time understanding these concepts and configuring the optimum hardware for the task.

January-2006

In the past month I have worked on solidifying the project outlines for the ice-phobic materials project by reviewing the literature on the modeling of ice surface. For that purpose I have analyzed various types of crystal forms of ice. I built the unit cell for hexagonal ice (I_h), so that as soon as the necessary AMBER modeling program is installed on the workstation I can replicate the unit cell to build the simulation box. This ice structure will be essential for the future simulation work, where the interactions between a candidate ice-phobic material and the ice surface will be investigated.

I also worked with Capt Kris Hardy on a LDF proposal. This proposal is based on the modeling and simulation of the ice-phobic materials project. Specifically, the adhesive interactions between ice and other surfaces will be investigated. These interactions between certain chemical groups are proposed to provide a guideline in designing ice-phobic materials in the laboratory. Additionally, modeling the binding of ice to an antifreeze protein will be performed. This will provide an insight into how the ice formation problem is solved in nature which in turn will provide clues as to how this problem may be solved via synthetic methods. Therefore, how they function can be used to design biomimetic coating systems with inherent anti-icing capability.

February-2006

In the past month I dedicated a considerable part of my time to setting up my Linux workstation. I worked with a computer support specialist for installation of Linux operating system as well as the following tools: Intel Math Kernel Libraries, FFTW libraries, MPICH parallel processing libraries, Intel C/C++ compilers, Intel Fortran compiler, AMBER molecular dynamics simulator, LAMMPS molecular modeling software, VMD visualization software, SPDBV modeling tool and XMGRACE scientific graphics software. I have tested all of this software. Particularly, I modeled a water box of ~600 water molecules using Tip4p and Tip4p/Ice water potentials and ran a test simulation at 300 K. The purpose of this modeling and simulation effort was two folds. First, I checked the AMBER for correctly running and benchmarked its performance on the workstation. Secondly, I wanted to evaluate the qualities of

the water potentials for reproducing certain properties such as density. Tip4p/Ice water potential is particularly important as it has been shown to reproduce crystallization into ice 1h phase at a temperature very close to the experimental observation. Therefore, I expect this potential to be at utmost importance for the ice-phobic materials research.

I also improved the ice 1h crystal I created previously. In addition to the positions of the oxygen atoms that has to satisfy the experimentally determined unit cell for ice 1h, the positions of the hydrogen atoms is also important. Namely, there is randomness in the hydrogen bonding. This randomness has to satisfy the "ice rules" determined by Bernal and Fowler. Additionally, the unit cell has to have zero net dipole moment and minimal net quadrupole moment. I implemented the results of a work by Hayward and Reimers so that all these requirements are met without having to go through time consuming Monte Carlo simulation to create the unit cells. This implementation is realized by a Fortran code I developed using GNU Fortran77. The resulting unit cells can directly be used for any future modeling studies that involve ice 1h.

A tertiary effort that I engaged in the past month was to acquire the best performance/price for a Beowulf cluster that we would like to purchase for the modeling work in AFRL/MLBT. As a result of this effort we agreed on a deal with an established vendor that provides us with the most economical package with equivalent product specifications and with on site maintenance that other vendors would not provide. I am confident that the modeling effort at MLBT will benefit substantially from the acquisition of this Beowulf cluster.

March-2006

In the past month, I have modeled a polyurethane (the main constituent in topcoat of an aircraft paint) slab in order to create the surface on which the ice will adhere and the adhesive interactions of will be studied. The molecule used in the modeling is a dimer of a product of the reaction of m-Phenylene diisocyanate with ethylene glycol. This molecule has been chosen for its simplicity in order to evaluate the success of the force field and the simulation protocol. While AMBER molecular dynamics program package has shown that it is capable of modeling and simulating the amorphous polyurethane system at the realistic density successfully, it lacks some features that enable conveniently modeling of a two phase system such as ice and polyurethane. Therefore, my current effort is to incorporate LAMMPS molecular modeling package for modeling the interface. I developed programming codes in Fortran 90 for the following purposes. First codes that make AMBER coordinate and topology files portable to

LAMMPS environment and vice versa. Then programs that analyze output from LAMMPS simulations and calculate averages and standard deviations for several quantities and plot the results in graphs automatically.

A second Linux workstation to be used in simulations has recently become available. As I have done for the first workstation I have been working with a computer support specialist for installation of Linux operating system as well as the following tools: Intel Math Kernel Libraries, FFTW libraries, MPICH parallel processing libraries, Intel C/C++ compilers, Intel Fortran compiler, AMBER molecular dynamics simulator, LAMMPS molecular modeling software, VMD visualization software, SPDBV modeling tool and XMGRACE scientific graphics software. I also worked networking two workstations so that the files will be transferred easily back and forth. The acquisition of this second computer will reduce the overall simulation time.

April-2006

I have modeled an isocyanurate molecule (Figure a) and an oligomer of polyester polyol (Figure b). The crosslinking reactions of the two molecules produce crosslinked polyurethane; the type that is commonly used in aircraft topcoats. I have then developed FORTRAN code that creates a simulation box of binary blends on a cubical lattice. Using this initial configuration created by this program I have performed equilibration simulations of isocyanurate and polyester. Using this equilibrated structure I have built another simulation box of the topcoat (isocyanurate and polyester) and the ice crystal. This initial configuration was further equilibrated and the ice-topcoat interface was obtained (Figure c). Next, I will begin working on calculating the energy of adhesion.

For the purpose of making crosslinked polyurethane thus modeling of a more realistic coating system, I have also been working on the modeling the crosslinking reaction. As reactions are not supported by simulation software, it was necessary for me to develop a programming code that performs this task. I have completed writing a code that can react given two atoms. Now, I will be working on extending the code so that it can perform a search in the simulation box, determine the pairs of the closest reacting groups and then perform the crosslinking reaction.

May-2006

<u>Adhesion of Ice on Coating Surfaces</u>

I have completed developing the crosslinking code "xlinker". The resulting over 1300 line long code will likely be an indispensable tool for creating crosslinked coating systems towards the modeling and simulation efforts in the paints and coatings group. The main function of the code is to determine the candidate reacting pairs and carry out the reactions. In doing this it sorts the reacting pairs with respect to their closeness thus closer pairs are given priority in the order of reaction. From the modeling point of view, the reaction of a pair of reacting groups mean that a set of changes occur on several atoms in the reacting molecules. These modifications include change of atom types, bond types, angle types and dihedral angle types. Additionally, some existing bonds, angles and dihedrals removed and new ones created.

An important feature of the code is that it performs crosslinking reaction of molecules in the primary simulation box with their images. Therefore, one can build crosslinked molecules with infinite length in any of the three dimensions. The modeled system therefore becomes very similar to the real systems. Figure (a) shows a two dimensional projection of a crosslinked molecule that is infinite in x and y directions.

The crosslinked system needs to be characterized in order to know the micro-scale architecture of the crosslinked molecules. The code performs a complete analysis and reports a wide set of information including density of crosslinking reactions, percentage of reactions, number of newly formed chains and their size, the members of newly formed chains, which reactive group in which molecules is linked with which other groups etc.

Currently I am running simulations of crosslinked polyurethane-ice interface. As these simulations finish I will extract the adhesion energies between polyurethane and ice.

<u>Tunable Adhesion</u>

We have recently initiated a project on the adhesion strength and mechanisms of single polymer chains with polar end groups on various surfaces within the context of tunable adhesion. The computer modeling of the system by MD simulation enables to obtain the force-displacement curve which then helps us to understand the non-covalent interactions between surfaces and candidate molecules for tunable adhesion. This modeling effort will be carried out along with scanning probe microscope (SPM) experiments. While the SPM experiments helps to validate the simulation results, the computer modeling enables to perform studies of several

molecules with varying architectures and end groups that are not available commercially and very difficult to synthesize in the lab. Therefore, the computer simulation and the SPM experiments will synergistically provide some insight into the molecular interactions leading to adhesion.

I have built a pair of gold crystal surfaces. One of them is the substrate and the other one is the SPM probe. I adapted a new potential function along with its force field (Dreiding FF) in order to correctly predict gold-organic molecule interactions. I have run a simulation in LAMMPS where the gold substrate was kept stationary whereas the probe was displaced at a constant speed. The polyethylene chain with thiol groups at the end was sandwiched between the gold surfaces. This configuration (Figure (b)) mimics SPM experiments so that the results of the simulation can be compared with the experiments. My current effort is to calculate the force on the golden probe that is imposed by the polymer chain as the probe moves upwards.

June-2006

I have continued working on the tunable adhesion project. In addition to the single chain configuration, I have created a self assembled monolayer (SAM) configuration. Accordingly, I modeled a SAM made up of 1,4-Benzenedimethanethiol (BDMT) and then placed it between a couple of gold substrates (see Fig. 1). Based on experimental and theoretical evidence I placed thiol groups on a ($\sqrt{3} \times \sqrt{3}$)-R30° triangular lattice on a surface of Au (111). The preliminary equilibration simulations of the modeled system showed that the BDMT molecules oriented as to from a herring-bone pattern as shown in Fig. 2 (inline with experimental evidence). Next effort will be to perform the simulations of AFM experiment on the system and calculate force-displacement curve.

I have authored computer modeling part of an AFOSR proposal based on the tunable adhesion project. Basically, we proposed to reveal adhesion mechanisms by combining data from the atomic force microscope (AFM) and the molecular dynamics simulations.

I have attended a three day workshop (2006 AFMC Deicing Workshop) held in WPAFB. I prepared a report based on the workshop to be submitted to my government sponsor.

July-2006

I have continued working on the tunable adhesion project. I performed multiple computer simulations of Atomic Force Microscope (AFM) experiment for 1,4-Benzenedimethanethiol (BDMT) in the single molecule and the self assembled monolayer (SAM) configurations. I

obtained the force-distance curves which is the main objective of this work. Currently, I am waiting for input from the actual AFM experiments to compare the simulation results to those obtained from the experiments.

I have worked on incorporating the visualization of the computer simulations to the evolution of the force-distance curve in the real time. Namely, my objective has been to display how the force imposed on the AFM tip by the BDMT molecules progresses as a result of approaching the tip towards the BDMT molecule/s. For this purpose I taught myself a scripting language (TCL) that can do the job efficiently and easily. The resulting TCL code inputs the data from the visualization software (VMD) and stream it to the to the graphics plotting tool (XMGRACE) in the real time. The code then converts the collection of resulting images into a movie format (mpg) that can be displayed on any type of computer. The outcome of this effort enables presenting the simulation results clearly by combining the qualitative results to the quantitative ones in the real time. Snapshots taken from the created movies for the single molecule and SAM configurations are shown in Figures 1 and 2, respectively.

August-2006

I have continued working on the tunable adhesion project. Previously, I had written a "tcl" script that calculates the three angles (θ, ψ, ϕ) that determine the conformation of BDMT molecules and the distribution functions for each of these three angles. In an attempt to carry out similar analyses for other self assembling molecules, I modeled biphenyldithiol (BPDT), benzylmercaptan (BM), 4-nitrobenzenethiol (NBT), thiophenol (TP), 4-methylbenzenethiol (TT) and 4-methylbenzylthiol (XT). I am currently working on obtaining the equilibrium configurations of the self assembled monolayers (SAMs) of these molecules.

Another point of interest for this study is the determining the positions (fcc, hcp or bridge) of sulfur atoms at the bottom of self assembling molecules on the Au (111) surface. For this purpose I wrote a "tcl" script that determines the position of each of 270 sulfur atoms on the gold surface and tracks it throughout the course of the molecular dynamics simulation. Having that information, with the FORTRAN code I wrote, one can determine the correlation function for each possible site (fcc, hcp or bridge). This function shows on average how much time a self assembling molecule spends on each of the site.

September-2006

I have continued working on the tunable adhesion project. Previously, I had written a "tcl" script that calculates the three angles (θ, ψ, ϕ) that determine the conformation of BDMT molecules and the distribution functions for each of these three angles. In an attempt to carry out similar analyses for other self assembling molecules, I modeled benzylmercaptan (BM), 4-nitrobenzenethiol (NBT), thiophenol (TP), 4-methylbenzenethiol (TT) and 4-methylbenzylthiol (XT) (see Fig 1). I am currently working on obtaining the equilibrium configurations of the self assembled monolayers (SAMs) of these molecules.

Another point of interest for this study is determining the positions (fcc, hcp or bridge) of sulfur atoms at the bottom of self assembling molecules on the Au (111) surface. For this purpose I wrote a "tcl" script that determines the position of each of 270 sulfur atoms on the gold surface and tracks them throughout the course of the molecular dynamics simulation. Having that information, with the FORTRAN code I wrote, one can determine the correlation function for each possible site (fcc, hcp or bridge). This function shows on average how much time a self assembling molecule spends on each of the site (see Fig 2).

I also wrote a "tcl" script to calculate the distance between the sulfur atom at the bottom of self assembling molecules and its 3 nearest gold atoms. I compared this data to the results from Density Functional Theory methods and observed a very good correspondence.

October-2006

I have been working on the "adaptable adhesion" project with an emphasis on modeling the self-assembled monolayers (SAMs). In addition to previously modeled SAM of 1,4-Benzenedimethanethiol, I modeled and obtained the equilibrium configurations of SAMs for benzylmercaptan, biphenyldithiol, thiophenol, 4-methylbenzenethiol and 4-methylbenzylthiol on Au (111) surface. I have performed various analyses on the SAMs in order to characterize and understand their conformational and dynamical characteristics. Specifically, I completed writing codes and scripts to obtain quantities including:

- distribution functions of three angles (θ, ψ, ϕ) that determine the conformation of self-assembling molecules
- positions (fcc, hcp or bridge) of sulfur atoms of SAMs on the Au surface
- time dependent correlation functions for each possible site (fcc, hcp or bridge) (see Figure 1)

- distance between the sulfur atom of self assembling molecules and its 3 nearest gold atoms

- mean square displacement (msd) for self-assembling molecules (see Figure 2)

Based on the outcome of these analyses, I am currently working on writing a paper to be submitted to a scientific journal.

I also attended a 3-day workshop on scientific software development at Ohio Supercomputer Center (Columbus) in October 24 - 26, 2006.

November-2006

I have been working on writing an article based on my modeling results of the self-assembled monolayers (SAMs). I completed "model" and "simulation protocol", sections while "results" and "discussion" sections are near complete.

I have also been working on configuring the new Beowulf cluster that I now have access to. I am working with the cluster vendor and the computer support in installing necessary software and resolving various configuration issues.

An additional effort was on the call for Statement of Need on "Scientific Understanding of Non-chromated Corrosion Inhibitors Function" by Strategic Environmental Research and Development Program (SERDP). I have done preliminary literature search on the matter and proposed some ideas to approach the problem.

December-2006

I have been working on writing an article based on my modeling results of the self-assembled monolayers (SAMs). I now completed the introduction, results and discussion sections in addition to the model and simulation protocol sections. I am planning to complete the paper within this coming month.

I worked on composing two LDF (Laboratory Director's Fund) proposals with Dr. Alex Khramov.

First proposal is titled: *"Controllable nano-structured interface based on self-assembled monolayer and gold nano-particles".* We proposed to create a hierarchical structure with controllable interfacial properties by sandwiching a SAM between a gold surface and a layer of gold nano-particles. Our approach is based on versatile and well-developed chemistry of thiol-functionalized SAMs on a gold surface and thiol-stabilized gold nano-particles. In addition to the

experimental approach, we plan to develop atomistic models of an ordered and a disordered SAM sandwiched between Au (111) layers.

Our second proposal is titled: *"Surface modification and patterning by grafting molecular loops of alkylene-bridged bis-silanes"*. The goal of this proposal is to achieve effective surface modification of a metal substrate by anchoring alkylene-bridged bis-silanes to the surface thus creating interfacial structure that consists of molecular loops extended out of the surface. Moreover, we will perform molecular dynamics simulations in order to elucidate the thermodynamic as well as the structural mechanisms involved in this surface modification process.

January-2007

I have completed the article based on my modeling results of conformational and dynamical behaviors of the self-assembled monolayers (SAMs). It is currently being internally reviewed. I plan to submit it to *Langmuir*.

Our proposal with Dr. Alex Khramov entitled: *"Controllable nano-structured interface based on self-assembled monolayer and gold nano-particles"* qualified for the second step of the selection process. Thus, I worked on composing an extended proposal that was re-submitted to the LDF (Laboratory Director's Fund) committee.

In addition to my previous simulations for ordered SAMs, I modeled a disordered layer of benzenedimethanethiol (BDMT) on a Au(111) surface. Subsequently, I performed simulations of AFM experiment on the disordered surface. The analyses for this simulation results will reveal the role of ordering in adhesive function of self assembling molecules between Au layers.

February-2007

I initiated a new project on modeling of self-healing polymers. The first stage of the project involves using a course-grained approach in modeling the cross-linked polymer system. I developed FORTRAN codes that form the initial structure of reactants which will form the cross-linked system. Additionally, I am working on developing a scheme that *dynamically* cross links the reactants by using home developed *x-linker* code and communicating with LAMMPS molecular simulator.

I started preparing my presentation to be presented at ACS National Meeting on March 26, 2007.

I attended a Python Programming workshop on 21 February, 2007 at Ohio Super Computer Center.

March-2007

I continued the project on self assembled monolayers as a part of more general effort on tunable adhesion project. I performed substantially longer 10 ns long simulations for six aromatic thiol molecules. I recalculated some quantities such as *mean squared displacement* and *site-correlation functions* with the larger set of data (Fig. 1). I incorporated this data into the paper that is to be sent to Langmuir after our internal review.

I continued the work on a course-grained approach in modeling the crosslinked system for self-healing project. I improved the FORTRAN code that form the initial structure of reactants which subsequently forms the crosslinked system and the scheme that *dynamically* cross links the reactants by using the *x-linker* computer code and, by communicating with LAMMPS molecular simulator. The next step is to perform uniaxial stretching simulations and to calculate the stress-strain curves.

I attended a 5 day long 2007 American Chemical Society National Meeting in Chicago, where I presented a talk entitled "Molecular Dynamics Simulation Study of Conformational and Dynamic Properties of Self-Assembled Thiol Monolayers on Au".

April-2007

I continued the work on the course-grained approach in modeling the crosslinked system for self-healing project. The FORTRAN code that forms the initial structure of reactants and subsequently forms the crosslinked system was improved. I updated the computational scheme that *dynamically* cross links the reactants by using the computer code *x-linker* and, by communicating with LAMMPS molecular simulator. Subsequently, I performed simulations where three modes of deformations (i.e. tensile, shear and compression) were applied to the polymeric *control network*. The stress response to the various modes of deformation was probed, which completes the first stage of the project. The next step will be the incorporation of ionic cross linking points to the control network (i.e. creating *ionic network*). The comparisons of the stress-strain characteristics for the *control network* and the *ionic network* will be utilized to quantitively assess the self-healing potential of the *ionic network*.

May-2007

I have worked on a talk was presented at CERMACS 2007 May 20-23, 2007 entitled: "Exploring conformations and dynamics of self-assembled thiol monolayers on Au by molecular dynamics simulations."

I have worked on an abstract for an invited talk to be presented at SAMPE Fall Technical Conference, October 29-November 1, 2007 entitled: "Adding Self Healing Character to Polymeric Networks via Ionic Bonds: A Coarse-Grained Molecular Dynamics Simulation Study." This talk will be based on our work where we adapted a coarse-grained representation in modeling of the network structure which was achieved by dynamically crosslinking the reactants. It involves our results for the stress-strain curves after imposing various forms of deformation and measuring their stress responses.

I also worked on finalizing the journal article that I submitted to Langmuir after the internal review.

I have been doing technical supervising for a summer hire on the self-assembled monolayer research.

June-2007

I have been working towards a paper to be submitted to SAMPE for the Fall Technical Conference. This paper entitled "Adding Self Healing Character to Polymeric Networks via Ionic Bonds: A Coarse-Grained Molecular Dynamics Simulation Study." is based on the work where a coarse-grained representation was adapted in modeling of the network structure which was achieved by dynamically crosslinking the reactants. For this purpose, I have been performing simulations of various forms of deformation and measuring their stress responses in order to obtain the stress-strain curves. I have also been doing calculations on various properties based on the simulation results.

I have been doing technical supervising Sheena Neely on the self-assembled monolayer research.

I worked with computer support in configuring one of the Linux workstations. We installed the operating system, compilers and various modeling and simulation software and tools.

July-2007

We are initiating a collaborative work with Brian Hinderliter at North Dakota State University on modeling and simulation of coating systems. As an initial step, I started reviewing the literature on appropriate atomistic force fields and coarse-graining a force field for polymer networks.

I have been researching software that performs quantum chemistry calculations and that visualizes the models and the outputs from the calculation. We acquired Gaussion 03 quantum chemistry software. I also evaluated "Molekel" and "gOpenMol" visualization tools. The objective is to add quantum level (*ab initio*) modeling capability to our modeling resources.

I have been supervising the summer researcher Sheena Neely as a technical point of contact on the self-assembled monolayer (SAM) research. I helped her in building the models, running the simulations, performing the analyses on linear alkanethiol SAMs. I also advised her during preparation of a technical paper and a presentation.

August-2007

I have been working on coarse-grained modeling of highly cross-linked polymeric networks towards the self-healing polymeric networks project. The previous system size was extended from 4,000 beads to 100,000. This increase aims to obtain a more representative and accurate model as well as less scattered data for properties such as stress-strain curves and toughness. The cross-linking procedure, which I previously designed, results in a very high cross-linking density of about 98%. In addition, the degree of ionic pairs was increased by 50%. I am currently running equilibrium simulations of the system that will be followed by deformation simulations.

Another focus of my efforts has been obtaining the force-distance curves for self assembled monolayers (SAMs). I intend to model SAMs of benzenebiphenyldithiol (BPDT) at three different possible phases: *ordered standing up, ordered lying down and disordered*. In my previous work I had modeled the *ordered standing up* phase correctly. Therefore, I have been working on modeling the *ordered lying dow*n phase. As experimental data on this particular phase is missing, its modeling has been intricate. I have recently managed to resolve the relevant issues and obtained the model. I am currently working to model the *disordered* phase.

September-2007

I have continued working on coarse-grained modeling of highly cross-linked polymeric networks towards the self-healing polymeric networks project. After building of a system with 100,000 beads and obtaining equilibrium structure, I have been working on optimizing the simulation parameters for deformation of the system in different modes. The test simulations have shown that the new set of parameters produce stress-strain curves in tensile and shear modes with desired consistency and accuracy (see Figure). In addition, another set of systems with varying degree of ionic cross-linking points have been created. The objective is to understand the effect of ionic cross-linking density on the mechanical and self-healing properties. I am currently working on a script that will run a series of simulations automatically on a supercomputer.

October-2007

I have worked on completing the simulations for the self-healing polymeric networks project. Stress-strain curves were obtained after exposing the standard model and ionic model to three different modes of deformations at higher strain rates. The results showed the expected enhancements in mechanical properties, particularly in impact resistance, were observed. The simulations for slow deformation rate are being run.

I worked on preparing a talk in Computational Materials Science session at SAMPE Fall Technical Conference that I delivered on Oct 31st.

I am currently working on an invited talk at the Department of Chemical & Materials Engineering in University of Cincinnati on Nov 8, 2007.

November-2007

I have been working on creating self-assembled monolayers of biphenyldithiol (BPDT) in lying-down as well as standing-up configurations. In addition to the ordered monolayers I have created a disordered thin film of the same compound. I have performed computational AFM experiments to obtain the force-distance curves on the three different phases. The objective is to compare the force-distance behavior for the different surfaces.

I have presented an invited talk at the Department of Chemical & Materials Engineering in University of Cincinnati on Nov 8, 2007.

I have authored a short paper entitled "Course-grained molecular dynamics simulations of self healing polymeric networks", for a presentation at 6th International Conference on Mechanics of Time-Dependent Materials.

December-2007

I have continued working on studying self-assembled monolayers of biphenyldithiol (BPDT) in lying-down as well as standing-up configurations. The computational AFM experiments have shown that the structure of monolayer has a significant impact on the adhesive character of the surface.

I have started writing a full paper to be submitted to the Mechanics of Time Dependent Materials Journal. This paper will be based on the coarse-grained molecular dynamics simulations of self-healing polymeric networks.

I have also pursued an exploratory research to understand the effect of directional anisotropy on adhesion. I used a coarse-grained approach to model a cross-linked body with a unique shape that is expected to provide anisotropy.

January-2008

I have continued an exploratory research to understand the effect of directional anisotropy on adhesion that is seen in gecko foot. I used a two-dimensional coarse-grained approach to model a cross-linked parallelepiped body with a 50° tilt. This shape is intended to mimic the type of anisotropy that appears to be the underlying mechanism in gecko's adhesion-release ability to surfaces. Computer simulations of detachment experiments at varying detachment directions were carried out. Early results have shown a qualitative agreement with experimental measurements of directional adhesion for a similar system by Guduru at Brown University.

I have completed writing a full paper to be submitted to the *Mechanics of Time Dependent Materials Journal*. This paper is based on the coarse-grained molecular dynamics simulations of self-healing polymeric networks and it addresses the effect of addition of ionic pairs into the network on time dependent mechanical properties.

February-2008

I have been working on organizing the results for the study of computational AFM experiments on self-assembled monolayers of biphenyldithiol (BPDT). The results of force-distance measurements in standing-up, lying-down, disordered configurations are being

compiled for a manuscript. An additional case when the AFM tip was coated with residual dithiols prior to the approach and withdrawal stages in the AFM simulation was studied. I have started writing the manuscript for a possible submission to Langmuir.

I have modeled another cross-linked network system for the self-healing polymeric networks project in order to validate our earlier results of stress-strain curves after applying different modes of deformation.

I provided input for the TRB review of "Adaptive & Active Composite & Hybrid Materials Program". I summarized the computational modeling effort and the current status in RXBT in regards to the adaptable adhesion and self-healing materials projects. In addition, I compiled the input provided from other researchers working on other aspects of the program to be submitted in the write-up for the review.